Contrib Mineral Petrol (1996) 124: 273–290 

I.S. Puchtel · A.W. Hofmann · K. Mezger · A.A. Shchipansky · V.S. Kulikov · V.V. Kulikova

# Petrology of a 2.41 Ga remarkably fresh komatiitic basalt lava lake in Lion Hills, central Vetreny Belt, Baltic Shield

Received: 8 December 1995/Accepted: 26 March 1996

**Abstract** In the central Vetreny Belt, southeastern Baltic Shield, an areally extensive 110 m deep lava lake is exposed consisting of remarkably fresh differentiated komatiitic basalt. During eruption, the liquid had a temperature of 1380–1400 °C and contained ~ 15% MgO. The lava ponded in a large topographic depression soon after eruption. The differentiation of the lava lake was controlled by settling of transported olivine and chromite phenocrysts and caused the origin of prominent internal layering. The last portions of the trapped liquid crystallized at temperatures of 1250–1070 °C. A Sm-Nd isochron of 2410 ± 34 Ma for whole rock samples, olivine, augite and pigeonite separates from the lava lake provides a reliable estimate for the time of formation of the uppermost sequences in the Vetreny Belt. This age is in good agreement with the Sm-Nd and Pb-Pb isochron ages of 2449 ± 35 and 2424 ± 178 Ma for the volcanic rocks from the same stratigraphic level in the northwestern Vetreny Belt. Modeling of Nd-isotopes and major and trace elements shows that the komatiitic basalts at Lion Hills may have had a komatiite parent depleted in highly incompatible elements. It can be shown that this initial liquid was contaminated by 7–9% of Archaean upper crustal material from the adjacent Vodla and Belomorian Blocks *en route* to the surface thus acquiring the observed geochemical and isotope signatures including relative enrichment in Zr, Ba, and LREE, negative Nb- and Ti-anomalies and εNd(T) of − 1.

I.S. Puchtel (✉) · A.W. Hofmann · K. Mezger
Max-Planck-Institut für Chemie, Postfach 3060, D-55020 Mainz, Germany

I.S. Puchtel
Institute of Ore Deposit Geology, Petrology, Mineralogy and Geochemistry (IGEM), Russian Academy of Sciences, Staromonetny per. 35, 109017 Moscow, Russia

A.A. Shchipansky
Geological Institute (GIN), Russian Academy of Sciences, Pyzhevsky per. 7, 109017 Moscow, Russia

V.S. Kulikov · V.V. Kulikova
Geological Institute, Karelian Center of the Russian Academy of Sciences, Pushkinskaya 11, 185610 Petrozavodsk, Russia

Editorial responsibility: J. Hoefs

## Introduction

The results from integrated studies of mafic-ultramafic volcanic suites are generally regarded as the basis for modelling the evolution of the composition and physical state of the Earth's mantle and crustal reservoirs (e.g., Arndt 1986a; Chase and Patchett 1988; Condie 1989; Dupré and Arndt 1990; Galer and Goldstein 1991; Jochum et al. 1991; Nisbet et al. 1993; Abbott 1994). The ambiguity of interpretation of these results with respect to Archean settings is mainly caused by the inadequate state of preservation of the object of investigation due to the effects of hydrothermal alteration and polyphase metamorphism.

All komatiitic and associated mafic volcanic rocks are more or less altered. In some cases the primary minerals are replaced pseudomorphically, and the important details of morphology of original minerals can still be recognized precisely and thus the precursor igneous minerals can be readily identified. But in most cases, recrystallization becomes complete and little remains of the primary texture. This makes it difficult to infer even the original nature of the premetamorphic protoliths of these rocks. When studying the chemical composition of such rocks, it is necessary to penetrate the veil of serpentinization or evev worse, the dense fog of amphibolite and granulite facies metamorphism. Uniquely fresh by Archean standards, the komatiites from Alexo, Ontario (Arndt 1986b) and especially from Zwishavane, Zimbabwe (Nisbet et al. 1987; Renner et al. 1994) can be indeed regarded as the window that

allows a glance into the depths of the Archean mantle and helps us to understand the mechanisms of formation of the Earth's early crust.

In the present paper we report the results of detailed field, petrographic, geochemical and Nd-isotope studies of the remarkably well preserved early Proterozoic high-magnesian volcanic rocks from the Vetreny Belt in the southeastern Baltic Shield. The objectives of the research include: (a) field study of a large differentiated body of komatiitic basalt in order to reconstruct its original nature; (b) detailed examination of mineralogy, petrography and chemistry of minerals and main rock varieties across the complete section in order to deduce the composition of the initial and erupted magma and the factors that controlled its differentiation after emplacement; (c) Nd-isotope studies of bulk rocks and primary minerals in order to raise further the curtain concealing the enigmatic problem of the age of the Vetreny Belt voleanism.

## Geological background

In the southeastern Baltic Shield, three large early Precambrian structural and lithological units are juxtaposed. They include Archean amphibolite-gneiss-migmatite and granite-greenstone units, and a Lower Proterozoic volcanic-sedimentary unit. The Archean units are volumetrically dominant and constitute the Karelian granite-greenstone terrane, which occupies a total area of approx. 350000 km$^2$ (Fig 1).

About 2.5 Ga ago, the Archean continental crust of the Karelian granite-greenstone terrane underwent tectono-magmatic reactivation during the Karelian stage (2.5–2.1 Ga). This episode of reactivation was initiated by continental rifting, as evidenced by the deposition of conglomerates, quartzites and arkoses. Subsequently areally extensive mafic volcanic rocks of the Sumi-Sariola group erupted, followed by the emplacement of mafic-ultramafic layered intrusions and rapid sedimentation in fault-bounded shallow-water basins (Gaál and Gorbatschev 1987; Gorbatschev and Bogdanova 1993). Most of the Sumian-Sariolian rocks occur in NW-trending volcano-sedimentary belts, their deposition and magmatism being controlled by NW-trending rift-formed fault systems. One of these large belts the Vetreny Belt (Fig. 1) is the subject of this study. This belt can be traced from lake Vyg southeastward over a distance of more than 250 km; its width increases from 15 to 85 km. In the southeast, the Vetreny Belt plunges under the Paleozoic cover of the Russian platform, and extends further on to the southeast (Kulikov 1988). In the northeast, the Belt is separated from the Belomorian Block by the Northern deep fault zone. The southwestern contact of the Vetreny Belt with the Sumozero-Kenozero greenstone belt and the Vodla Block is also tectonic in character.

The early Proterozoic rocks of the Vetreny Belt are subdivided into six major suites (Fig. 1). The lowermost part of the sequence is represented by the terrigenous (quartzites) Toksha suite, andesites

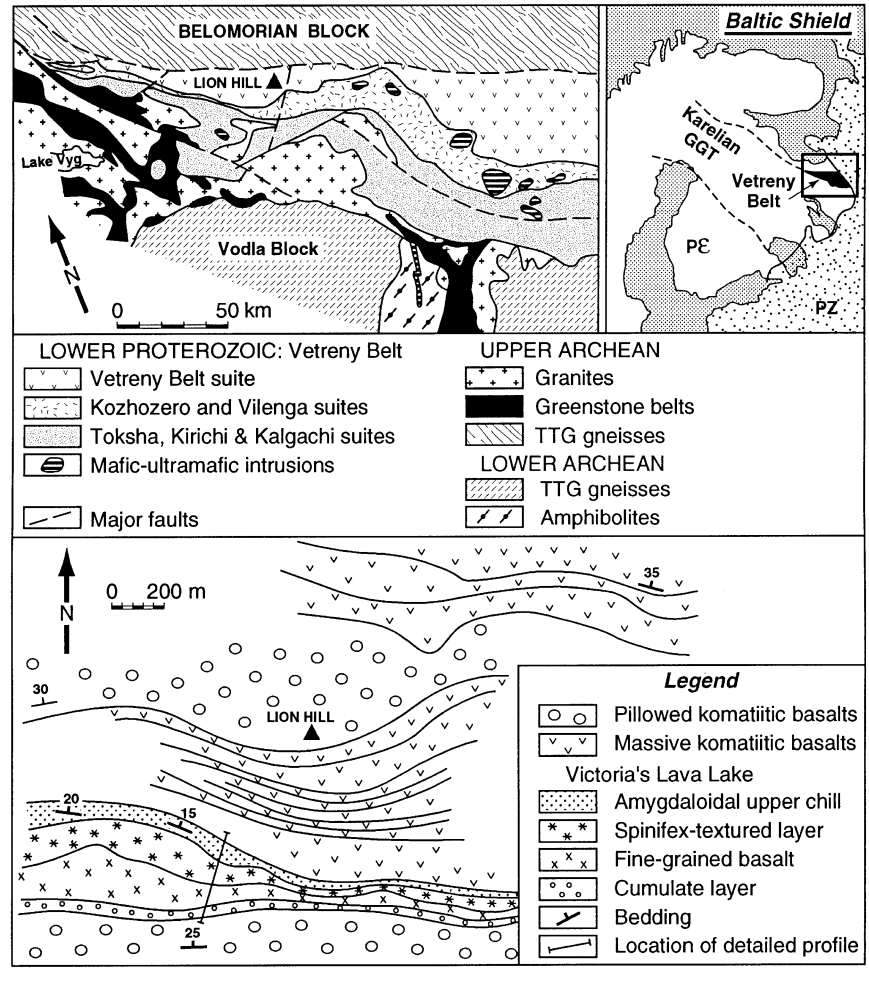


**Fig. 1** Geological sketch map of the Vetreny Belt. Geologic-petrographic map of the Lion Hills area

and basalts of the Kirichi suite and polymict conglomerates and sandstones of the Kalgachi suite. These are overlain by the terrigenous sediments and basalts of the Kozhozero suite, and further upward in the succession, by the tuffaceous and terrigenous Vilenga suite and the Vetreny Belt suite; the latter is composed entirely of komatiitic basalts. The total thickness of the early Proterozoic sequences in this area varies between 4 and 8 km (Kulikov 1983; Sokolov 1987).

This study focuses on the high-magnesian volcanic rocks from the Vetreny Belt suite in the Lion Hills area (Fig. 1). These rocks were recognized and described as high-magnesian basalts by Kulikov (1971) and Slyusarev and Kulikov (1973). Kulikov and Kalinin (1971) reproduced the chilled textures observed in these basalts experimentally and made an attempt to explain the mechanisms responsible for these spectacular textures. Almost at the same time these textures became referred to as spinifex textures (Nesbitt 1971).

In the Lion Hills area, lava flows are dipping consistently to the NNE at angles of 20 to 40°, and range in thickness from a few meters to several tens of meters. The metamorphic grade in the central part of the area surrounding Lion Hill does not exceed the prehnite-pumpellyite facies. The rocks in this area are well exposed and are characterized by the superb state of preservation of primary minerals. The northern slope of the hill is made up of massive and pillowed komatiitic basalts. On the southern side, regular lava flows of the same type are also exposed in addition to a thick differentiated lava unit. Based on field ralationships and petrologic observation this lava unit is interpreted as the remnants of an areally extensive and deep lava lake. After one of its disoverers we name this unit Victoria's lava lake.

This ancient lava lake was documented on the nearly vertical walls of a little canyon that cuts the lake across strike. The lake is gently plunging to the north at 15 to 30°, and can be traced along strike over a distance of more than 2.5 km; in the west and east it is covered by Quaternary glacial deposits. Its thickness decreases from 150 m in the western part down to 60 m in the eastern part of the hill; in the best exposed part within the canyon it is around 110 m deep. The rocks that make up this lava lake are characterized by a wide variety of structures and textures (Fig. 2). In general, the lake consists of four main units (from top downward): (1) scoria; (2) upper chilled margin; (3) spinifex zone, which includes the spinifex subzone proper and the subzone of a fine-grained basalt; (4) cumulate zone.

## Petrography of the lava lake

Before describing the petrography of the lava lake, it is necessary to make a few introductory statements concerning the terminology used throughout this paper. To describe crystals having a substantially larger size than those in the groundmass, the term

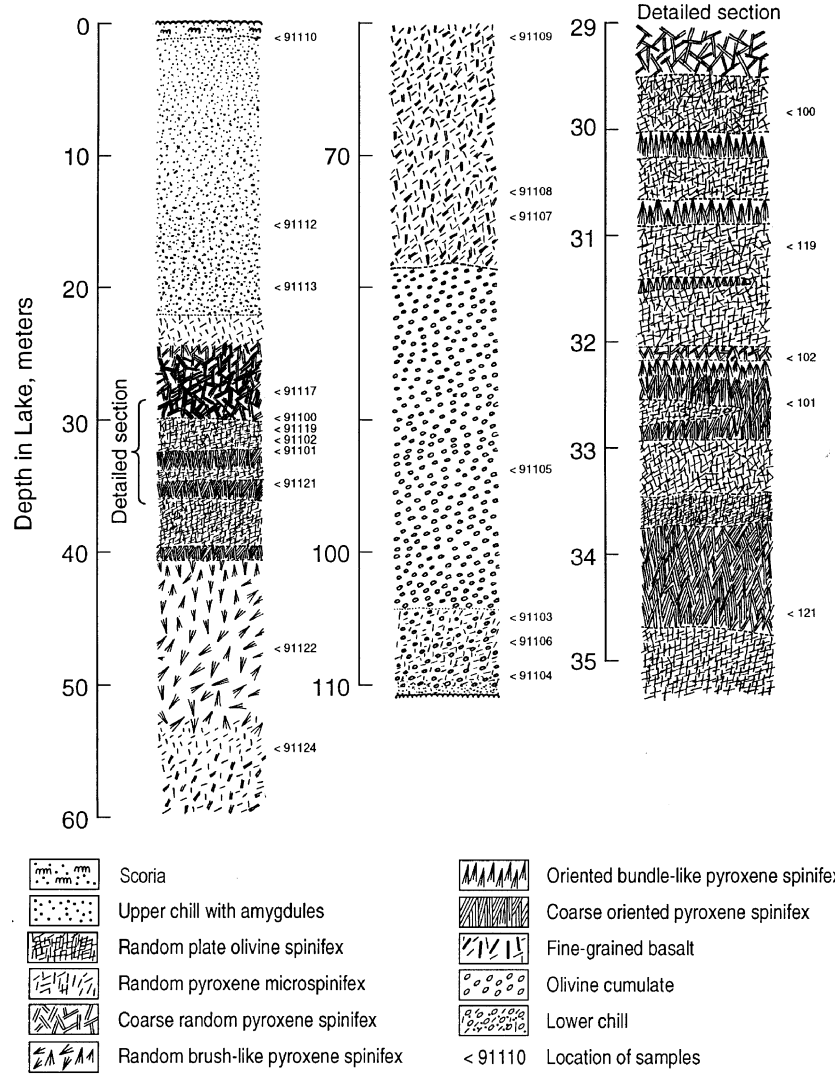


**Fig. 2** Detailed profile through Victoria's lava lake

phenocryst ( > 0.5 mm) and microphenocryst ( < 0.5 mm) are adopted. Individual olivine, pyroxene and chromite morphology was described using the terminology introduced by Lofgren et al. (1974) and Donaldson (1976, 1982). Among the olivines, three morphological types were distinguished: (a) solid euhedral equant to tabular crystals; (b) equant to elongate hopper (externally euhedral to subhedral but internally hollow and incomplete) crystals, sometimes with perceptible edge growth; (c) plate olivine. The pyroxene was documented as: (a) prismatic and blocky crystals; (b) columnar and acicular hollow crystals; (c) chain crystals; (d) plumose and feather-like crystals.

## Scoria

The scoria is a thin ( ~ 0.5 m) layer containing rounded and amoeboid to subangular lighter-colored clasts up to 2 cm in diameter cemented by cryptocrystalline basaltic material. The clasts consis of devitrified volcanic glass containing tiny solid euhedral and cruciform (euhedral core and snowflake-like overgrowths) chromite grains and serpentinized olivine crystals. The latter are subdivided into two groups: (1) small (0.1–0.3 mm) solid and incomplete equant euhedral microphenocrysts in clusters of 7–10 grains that make up about 15% of the rock by volume; (2) larger (0.6–2.5 mm) solid and rarely incomplete equant to subequant phenocrysts constituting some 10% of the rock.

## Upper chilled margin

In the upper chilled margin, olivine is almost completely serpentinized and is represented by both pheno- and microphenocrysts and a tiny mesh of hopper bladed crystals 0.1–1 mm in length, set in a brownish matrix after glass and constituting the olivine microspinifex texture (Fig. 3a). The chilled margin reveals a heterogeneous

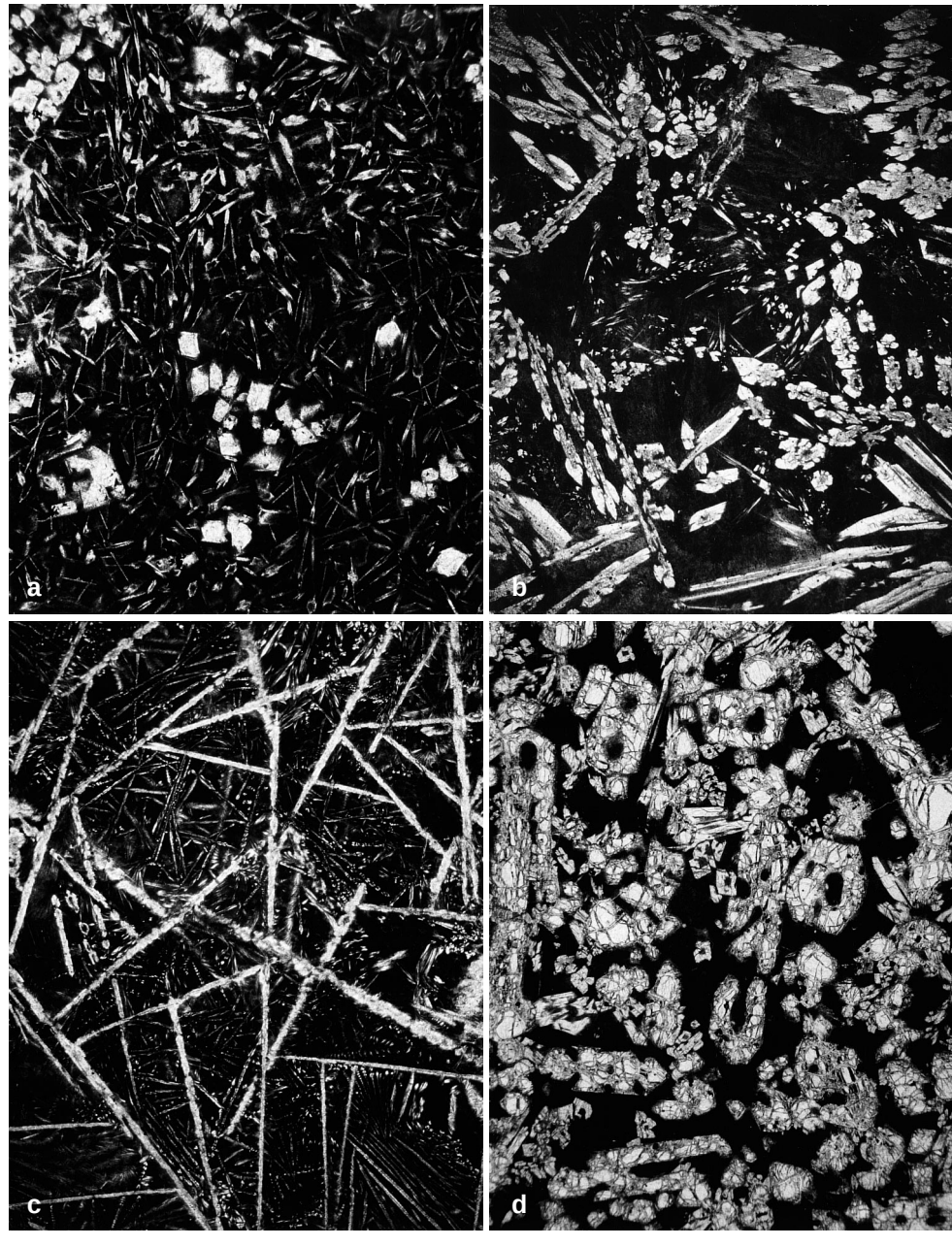


**Fig. 3a–d** Photomicrographs of representative types of rocks, plane-polarized light: **a** upper chilled margin, sample 91110, 5.8 mm across the photograph; **b** coarse random pyroxene spinifex layer, sample 91117, 11.6 mm across the photograph; **c** plate olivine spinifex layer, sample 91118, 11.6 mm across the photograph; **d** Olivine cumulate layer, sample 91105, 5.8 mm across the photograph. See text for explanations

texture owing to the presence of thin layers variably enriched in chlorite-serpentine-feldspar amygdules, 1–1.5 mm in diameter.

### Spinifex zone

The upper part of the spinifex zone is largely made up of a layer of coarse random pyroxene spinifex. It is characterized by development of long (up to 30 mm) and ~1 mm thick hollow columnar and chain zoned pyroxene crystals, and euhedral to subhedral hopper olivine crystals 2–7 mm long in a matrix of devitrified glass and plumose and chain pyroxene (Fig. 3b). The plate olivine spinifex is composed of thin (0.1–0.3 mm) plate olivine crystals up to 25 mm in length oriented nearly orthogonal to each other and imparting a cell-like structure to the rock (Fig. 3c). The cells are filled with devitrified glass and plumose and chain augite. The plate olivine spinifex layer contains thin (12–25 cm) bands of bundle-like pyroxene spinifex and thicker layers of coarse oriented pyroxene spinifex. In the bundle-like spinifex, acicular pyroxene crystals up to 70 mm in length are arranged in bundles, or sheaves nucleating at the upper contact of the layer and splaying downward. The groundmass consists of devitrified glass, plumose pyroxene and cruciform chromite. The oriented coarse pyroxene spinifex ("string beef" spinifex after Arndt et al. 1977) is characterized by the development of up to 12 cm long and 0.5–1 mm thick columnar zoned pyroxene crystals arranged roughly parallel to each other and subperpendicular to the top of the lake. The interstices are filled with devitrified glass, plumose pyroxene, cruciform chromite and tiny plagioclase laths.

The random brush-like pyroxene spinifex layer consists of columnar and chain pyroxene dominating over rare olivine platelets up to 15 mm in length immersed within aggregates after devitrified glass. Toward the bottom of the layer, olivine disappears, and the abundance and grain size of pyroxene decreases, the rock thus displays a microcrystalline texture and grades down into fine-grained basalt. The latter consists of tiny (0.5–2 mm) plagioclase laths and short-prismatic clinopyroxene. Cumulate zone.

The contact between the spinifex and cumulate zone is abrupt, with dramatic changes in mineralogy and textural relationships. The cumulate zone is subdivided into the olivine cumulate subzone proper and a basal subzone. The olivine cumulate is composed of two morphological types of olivine. The first type, which constitutes 3/4 of the whole olivine population, is represented by solid rounded, polyhedral or elongated crystals 0.2–2.5 mm in size. Often they reveal a lighter-colored core and darker edges. The second type is present in the form of hollow or incomplete crystals 0.4–3 mm in size. The internal parts of the crystals are filled with glass (Fig. 3d). Pyroxene occurs in the form of small (0.2 × 1 mm) incomplete long-prismatic and blocky, sometimes zoned crystals. Small euhedral chromite crystals are present as either inclusions in olivine, or dispersed in glass. The crystalline phases constitute 50–60% of the rock volume. The brownish glass is mostly isotropic indicating a very good state of preservation.

The basal subzone is distinct in having a crystalline matrix consisting of fine-grained pyroxene, tiny plagioclase laths and disseminated equant chromite. Embedded within the groundmass are solid rounded and euhedral olivine phenocrysts 0.4–2 mm in size (15–20% of the rock volume) and small (0.2–0.4 mm) skeletal or larger (0.5–2 mm) irregular pigeonite and augite grains, many of which contain rounded olivine as poikilitic inclusions.

## Analytical techniques

Mineral fractions were separated at the Geological Institute in Petrozavodsk. About 150 mg of pure high-Ca pyroxene and 300–500 mg of low-Ca pyroxene and olivine separates were then obtained at IGEM in Moscow by handpicking the ~99% pure concentrates.

Microprobe studies were carried out at the Mineralogisch-Petrographisches Institut, University of Cologne, using a Cameca Camebax electron microprobe. Operating conditions were 15 kV accelerating voltage, 20 nA beam current and integration time of 10 s per element. To obtain information on compositional zoning, traverses across mineral grains in steps of several tens of μm were performed, and 5 to 10 points were analyzed on some grains.

Chemical studies were undertaken on 150 g aliquots from 1–3 kg of fresh sample. Major element abundances were determined by X-ray fluorescence on fused glass pellets using a Philips PW-1404 at the Johannes Gutenberg University in Mainz; trace elements were analyzed on pressed powder pellets on the same XRF-machine. The REE concentrations were determined at IGEM in Moscow by isotope dilution mass-spectrometry using the method described by Thirlwall (1982) and modified by Zhuravlev et al. (1989). Accuracies are estimated as follows: major elements – 2 per cent for elements present in concentrations greater than 0.5%; trace elements – 5 per cent for Zr, Cr, V, Co, Ni and Ba; 10 per cent for Y and Sr; 20 per cent for Nb and Rb. Multiple analyses of the BCR-1 standard established the accuracy for La to be 2%, and for the remaining REE as better than 2%.

The Sm-Nd isotope investigations were carried out at the Max-Planck Institut für Chemie in Mainz following techniques described by Chauvel et al. (1985). Both Nd and Sm were run on a MAT-261 Finnigan mass-spectrometer under static mode. The total blank was 0.05 ng for Nd and 0.01 ng for Sm. The effects of fractionation during Nd runs were eliminated by normalizing to $^{146}Nd/^{144}Nd = 0.7219$. The $^{143}Nd/^{144}Nd$ isotope ratio measurements of the La Jolla standard during the period of data collection yielded a value of $0.511831 \pm 20$ ($2\sigma_{pop.}$; $n = 21$). All Nd-isotope ratios were bias corrected to the La Jolla standard $^{143}Nd/^{144}Nd = 0.511860$. Regression analyses followed the method of York (1966), and the error on the initial $\varepsilon_{Nd}$ value was calculated using the method of Fletcher and Rosman (1982). The analytical uncertainties used in the regression calculations were 0.2% for $^{147}Sm/^{144}Nd$ and for $^{143}Nd/^{144}Nd$, the $2\sigma_{pop.}$ value for the La Jolla standard corresponding to its external reproducibility. All errors on ages and initial isotopic ratios are quoted at $2\sigma$, or 95% confidence level. The Sm-Nd age was calculated using a decay constant for $^{147}Sm$ of $6.54 \times 10^{-12}\,a^{-1}$.

## Results

### Composition of minerals

Representative microprobe analyses of minerals and volcanic glass are given in Tables 1 to 4.

#### *Olivine*

In the upper chilled zone, only a few relict olivine phenocrysts remain unaltered. In the cumulate zone, however, olivine is remarkably well preserved and was therefore studied in more detail. In general, olivine composition is dependent on the size and morphological type of the crystals. Larger solid phenocrysts have a slightly more magnesian composition than microphenocrysts. Hopper crystals show the lowest forsterite content. Cores of larger phenocrysts are characterized by rather uniform compositions and a decrease in Fo content within thin outer rims; microphenocrysts and especially hopper grains reveal continuous normal zoning from the center toward the edges of the crystals.

**Table 1** Representative microprobe analyses of olivines from Victoria's lava lake. (*Hopp* hopper, *L* large, *S. Ph* small polyhedral olivine grains respectively)

| Sample no. | 91112 | 91112 | 91105 | 91105 | 91105 | 91105 | 91105 | 91105 | 91105 | 91105 | 91105 |
|---|---|---|---|---|---|---|---|---|---|---|---|
| Morphology | Hopp | Hopp | L. Ph | L. Ph | L. Ph | L. Ph | S. Ph | S. Ph | Hopp | Hopp | Hopp |
| Location | Core | Core | Core | Core | Rim | Rim | Core | Core | Core | Core | Rim |
| $SiO_2$ | 40.77 | 40.28 | 39.94 | 39.70 | 40.33 | 40.01 | 40.62 | 40.27 | 39.57 | 40.04 | 40.07 |
| $TiO_2$ | 0.030 | 0.000 | 0.025 | 0.002 | 0.012 | 0.000 | 0.008 | 0.026 | 0.000 | 0.002 | 0.000 |
| $Al_2O_3$ | 0.012 | 0.040 | 0.036 | 0.025 | 0.058 | 0.067 | 0.060 | 0.073 | 0.040 | 0.031 | 0.046 |
| $Cr_2O_3$ | 0.140 | 0.200 | 0.098 | 0.130 | 0.096 | 0.072 | 0.096 | 0.091 | 0.073 | 0.061 | 0.078 |
| FeO | 10.91 | 10.67 | 11.79 | 12.34 | 12.51 | 13.79 | 12.49 | 12.16 | 13.76 | 14.05 | 15.86 |
| MnO | 0.130 | 0.177 | 0.199 | 0.178 | 0.170 | 0.177 | 0.140 | 0.191 | 0.164 | 0.204 | 0.237 |
| NiO | 0.310 | 0.280 | 0.282 | 0.290 | 0.288 | 0.220 | 0.286 | 0.291 | 0.304 | 0.214 | 0.211 |
| MgO | 48.06 | 48.07 | 45.94 | 45.78 | 45.89 | 45.36 | 46.02 | 46.07 | 45.18 | 45.40 | 43.33 |
| CaO | 0.370 | 0.300 | 0.243 | 0.236 | 0.237 | 0.246 | 0.260 | 0.246 | 0.260 | 0.233 | 0.282 |
| Total | 100.7 | 100.0 | 98.54 | 98.68 | 99.59 | 99.94 | 99.98 | 99.42 | 99.35 | 100.2 | 100.1 |
| % Fo | 88.7 | 88.93 | 87.42 | 86.87 | 86.74 | 85.43 | 86.79 | 87.11 | 85.40 | 85.21 | 82.96 |

| Sample no. | 91105 | 91103 | 91103 | 91103 | 91106 | 91106 | 91106 | 91106 | 91106 | 91106 | 91106 |
|---|---|---|---|---|---|---|---|---|---|---|---|
| Morphology | Hopp | L. Ph | L. Ph | L. Ph | L. Ph | L. Ph | L. Ph | L. Ph | L. Ph | L. Ph | L. Ph |
| Location | Rim | Core | Core | Rim | Core | Core | Rim | Core | Core | Core | Core |
| $SiO_2$ | 39.63 | 40.38 | 40.91 | 40.14 | 40.00 | 40.51 | 40.26 | 40.19 | 40.07 | 39.80 | 40.12 |
| $TiO_2$ | 0.002 | 0.000 | 0.019 | 0.028 | 0.000 | 0.002 | 0.000 | 0.012 | 0.007 | 0.000 | 0.000 |
| $Al_2O_3$ | 0.028 | 0.056 | 0.040 | 0.039 | 0.017 | 0.029 | 0.018 | 0.052 | 0.060 | 0.038 | 0.063 |
| $Cr_2O_3$ | 0.088 | 0.077 | 0.073 | 0.064 | 0.096 | 0.048 | 0.043 | 0.067 | 0.101 | 0.111 | 0.116 |
| FeO | 16.40 | 11.67 | 11.75 | 13.59 | 10.81 | 11.22 | 12.22 | 10.98 | 11.15 | 11.26 | 11.47 |
| MnO | 0.283 | 0.191 | 0.106 | 0.181 | 0.143 | 0.180 | 0.176 | 0.141 | 0.179 | 0.112 | 0.181 |
| NiO | 0.225 | 0.304 | 0.332 | 0.283 | 0.223 | 0.222 | 0.249 | 0.300 | 0.247 | 0.341 | 0.288 |
| MgO | 42.49 | 46.71 | 47.42 | 45.18 | 47.46 | 47.91 | 47.72 | 47.86 | 46.73 | 47.22 | 47.76 |
| CaO | 0.271 | 0.211 | 0.236 | 0.237 | 0.220 | 0.158 | 0.191 | 0.229 | 0.259 | 0.238 | 0.229 |
| Total | 99.42 | 99.59 | 100.9 | 99.74 | 98.98 | 100.3 | 100.9 | 99.83 | 98.80 | 99.12 | 100.2 |
| % Fo | 82.21 | 87.71 | 87.80 | 85.56 | 88.67 | 88.39 | 87.44 | 88.60 | 88.19 | 88.20 | 88.13 |

In the upper chilled margin, hopper crystals have compositions of $Fo_{88.7-88.9}$. Due to the very small size of the relict grains, it was not possible to investigate the compositional zoning in the crystals. In the olivine cumulate subzone proper, cores of larger polyhedral grains have compositions varying from $Fo_{87.4-86.3}$ to $Fo_{85.4}$ at the margins. Small phenocrysts have a rather constant forsterite content of $Fo_{87.1-86.3}$. The compositions of hopper crystals vary from $Fo_{85.4-85.2}$ in the cores to $Fo_{81.7}$ at the rims. In the basal chill subzone, cores of large phenocrysts have the most magnesian compositions recorded in the cumulate zone ($Fo_{88.7}$) and are identical to the hopper grains in the upper chilled zone. Small phenocrysts show a wide range from $Fo_{87.8-86.7}$ in the cores to $Fo_{82}$ at the rims.

## *Pyroxenes*

The pyroxenes are compositionally similar to those from komatiite complexes elsewhere (Arndt et al. 1977; Arndt and Fleet 1979; Arndt 1986b; Renner et al. 1994). Skeletal blocky crystals from the groundmass of the olivine cumulate subzone proper are unzoned and correspond to high-Al (5.4–8.0% $Al_2O_3$) augite $Wo_{45}En_{44}Fs_{11}$–$Wo_{38}En_{46}Fs_{16}$. In the basal subzone, skeletal crystals of both low-Al (1.7–2.5% $Al_2O_3$) augite $Wo_{42}En_{49}Fs_{10}$–$Wo_{34}En_{52}Fs_{14}$ and magnesian pigeonite $Wo_4En_{75}Fs_{21}$–$Wo_{19}En_{64}Fs_{17}$ were documented. Tiny crystals of chain skeletal pyroxene from the plate olivine spinifex layer are, as a rule, unzoned and correspond to high-Al (5.4–7.1% $Al_2O_3$) augite $Wo_{45}En_{41}Fs_{14}$–$Wo_{36}En_{51}Fs_{13}$. In contrast, large columnar hollow crystals from the coarse random and oriented pyroxene spinifex layers are always zoned with pigeonite ($Wo_{11}En_{76}Fs_{13}$–$Wo_8En_{78}Fs_{14}$) cores, and outer portions composed of moderately Al-rich (2.2–5.2% $Al_2O_3$) augite $Wo_{30}En_{60}Fs_{10}$–$Wo_{40}En_{50}Fs_{10}$.

## *Chromite*

Two morphological types of chromite were documented. Cruciform skeletal crystals mainly occur in the spinifex zone, while solid equant euhedral grains are typical of the cumulate zone. Both types of chromite are similar and correspond to alumochromites. In the $Cr_2O_3$ versus $Al_2O_3$ and $TiO_2$ diagrams, the chromites

**Table 2** Representative microprobe data for clinopyroxenes from Victoria's lava lake (*Aug* augite, *Pig* pigeonite)

| Sample no. | 91105 | 91105 | 91104 | 91104 | 91106 | 91106 | 91106 | 91106 | 91106 | 91106 |
|---|---|---|---|---|---|---|---|---|---|---|
| Morphology | Prism | Prism | Prism | Prism | Prism | Prism | Prism | Prism | Prism | Prism |
| Composition | Aug | Aug | Aug | Pig | Pig | Aug | Aug | Pig | Aug | Pig |
| $SiO_2$ | 49.85 | 49.40 | 51.99 | 54.22 | 53.45 | 51.32 | 52.83 | 53.70 | 51.61 | 53.16 |
| $TiO_2$ | 0.594 | 0.796 | 0.639 | 0.235 | 0.310 | 0.759 | 0.395 | 0.242 | 0.551 | 0.239 |
| $Al_2O_3$ | 5.54 | 5.89 | 2.17 | 1.30 | 1.26 | 1.90 | 1.70 | 0.91 | 1.92 | 1.13 |
| $Cr_2O_3$ | 0.111 | 0.244 | 0.437 | 0.251 | 0.186 | 0.108 | 0.255 | 0.205 | 0.356 | 0.126 |
| FeO | 7.23 | 6.23 | 7.90 | 12.14 | 11.78 | 8.89 | 8.92 | 13.40 | 9.04 | 14.36 |
| MnO | 0.164 | 0.145 | 0.180 | 0.313 | 0.300 | 0.193 | 0.216 | 0.270 | 0.252 | 0.319 |
| NiO | 0.032 | 0.070 | 0.043 | 0.048 | 0.050 | 0.070 | 0.066 | 0.084 | 0.036 | 0.101 |
| MgO | 15.04 | 15.00 | 17.28 | 25.54 | 24.19 | 17.37 | 21.47 | 26.37 | 18.37 | 25.08 |
| CaO | 19.79 | 20.44 | 18.67 | 5.46 | 7.88 | 18.16 | 13.32 | 3.48 | 16.97 | 4.08 |
| $Na_2O$ | 0.181 | 0.221 | 0.220 | 0.022 | 0.113 | 0.242 | 0.135 | 0.053 | 0.189 | 0.070 |
| Total | 98.53 | 98.43 | 99.53 | 99.51 | 99.53 | 99.02 | 99.30 | 98.72 | 99.30 | 98.66 |
| Wo | 42.7 | 44.3 | 38.2 | 10.8 | 15.5 | 36.9 | 26.6 | 6.9 | 34.2 | 8.1 |
| En | 45.1 | 45.2 | 49.2 | 70.4 | 66.3 | 49.0 | 59.6 | 72.5 | 51.5 | 69.5 |
| Fs | 12.2 | 10.5 | 12.6 | 18.8 | 18.1 | 14.1 | 13.9 | 20.7 | 14.2 | 22.3 |
| Sample no. | 91118 | 91118 | 91118 | 91117 | 91117 | 91123 | 91123 | 91101 | 91101 | 91101 |
| Morphology | Chain | Chain | Chain | Colum | Colum | Colum | Colum | Colum | Colum | Colum |
| Composition | Aug | Aug | Aug | Pig | Aug | Aug | Aug | Aug | Aug | Pig |
| $SiO_2$ | 50.65 | 49.63 | 49.39 | 55.01 | 53.35 | 52.80 | 57.38 | 53.06 | 53.48 | 54.56 |
| $TiO_2$ | 0.594 | 0.418 | 0.520 | 0.115 | 0.350 | 0.416 | 0.412 | 0.186 | 0.250 | 0.127 |
| $Al_2O_3$ | 6.73 | 5.79 | 5.97 | 1.75 | 3.57 | 3.39 | 3.78 | 2.48 | 2.92 | 2.34 |
| $Cr_2O_3$ | 0.624 | 1.06 | 0.330 | 0.465 | 0.307 | 0.307 | 0.089 | 0.283 | 0.488 | 0.598 |
| FeO | 7.73 | 7.88 | 8.63 | 9.08 | 7.07 | 8.68 | 7.86 | 6.66 | 6.26 | 8.66 |
| MnO | 0.150 | 0.217 | 0.155 | 0.207 | 0.206 | 0.205 | 0.229 | 0.142 | 0.170 | 0.206 |
| NiO | 0.009 | 0.000 | 0.015 | 0.040 | 0.013 | 0.000 | 0.011 | 0.006 | 0.011 | 0.021 |
| MgO | 13.96 | 17.13 | 14.35 | 28.41 | 18.26 | 20.37 | 15.84 | 20.59 | 19.38 | 27.69 |
| CaO | 19.21 | 16.96 | 18.88 | 4.13 | 17.37 | 13.70 | 13.35 | 15.47 | 16.38 | 4.61 |
| $Na_2O$ | 0.187 | 0.199 | 0.177 | 0.041 | 0.215 | 0.167 | 0.214 | 0.146 | 0.229 | 0.073 |
| Total | 99.84 | 99.29 | 98.41 | 99.25 | 100.7 | 100.0 | 99.15 | 99.04 | 99.57 | 98.89 |
| Wo | 43.0 | 36.1 | 41.4 | 8.1 | 36.0 | 28.1 | 32.1 | 31.4 | 34.0 | 9.2 |
| En | 43.5 | 50.8 | 43.8 | 77.9 | 52.6 | 58.1 | 53.1 | 58.1 | 55.9 | 77.2 |
| Fs | 13.5 | 13.1 | 14.8 | 14.0 | 11.4 | 13.9 | 14.8 | 10.5 | 10.1 | 13.5 |

occupy the low-Cr and high-Al and high-Ti corners of the komatiite field distinguished by Zhou and Kerrich (1992), Herbert (1982) and Jan and Windley (1990), while in the $Cr_2O_3$ versus FeO plot they are almost outside the range of FeO contents observed in komatiites and in continental layered intrusions at given chromium abundances. Compared to chromites from the more magnesian counterparts elsewhere they are therefore enriched in $Al_2O_3$ and FeO and depleted in MgO.

### *Volcanic glass*

Glass was analyzed from the cumulate subzone proper and from the plate olivine spinifex layer in places where it shows the least degree of alteration and therefore represents the closest approximation to the composition of the latest portions of trapped liquid. As can be seen in Table 4, it displays a wide compositional range with $SiO_2$ varying between 49.3–55%, and MgO from 2.7–7.9%.

## Chemical compositions of the rocks

For chemical and Nd-isotope studies, 18 samples were collected along the detailed profile (Fig. 2). Major, trace, and rare earth element data normalized to 100% on a volatile-free basis are listed in Table 5 and shown in the variation diagrams Figs. 4 and 5. The MgO content ranges from 26.1% in the cumulate zone to 7.3% in the fine-grained basalt layer. In the upper part of the lake, the MgO abundances are rather uniform and change slightly from 14.7% at the top to 13.7% at the bottom of the upper chilled margin. The spinifex zone proper contains 10.3–8.8% MgO.

Most components show a strong correlation with MgO ($r = 0.99$–$1.00$ for Ti, Al, Zr, Y, V, Ni, and REE, and 0.97–0.98 for Ca and Sr) and vary in a manner entirely consistent with olivine fractionation. When plotted against wt% MgO, the analytical data fall on olivine control lines (Fig. 4), which intersect the MgO axes at $47.9 \pm 0.7\%$ ($2\sigma_{mean}$). Sample 91113 from the bottom of the upper chilled margin contains abundant

**Table 3** Representative microprobe data for chromites from Victoria's lava lake. All crystals analyzed are solid equant grains. (*ND* not detected)

| Sample no. | 91105 | 91105 | 91105 | 91105 | 91105 | 91106 | 91117 |
|---|---|---|---|---|---|---|---|
| $SiO_2$ | 0.14 | 0.76 | 0.08 | 0.10 | 0.09 | 0.04 | 0.06 |
| $TiO_2$ | 0.430 | 0.497 | 0.439 | 0.435 | 0.450 | 0.909 | 0.519 |
| $Al_2O_3$ | 13.16 | 13.62 | 13.95 | 13.17 | 13.73 | 8.86 | 14.99 |
| $Cr_2O_3$ | 46.46 | 46.25 | 47.25 | 46.63 | 47.40 | 45.89 | 43.67 |
| FeO | 35.21 | 34.05 | 32.81 | 33.48 | 32.70 | 38.36 | 36.18 |
| MnO | ND | ND | ND | ND | ND | ND | ND |
| NiO | 0.047 | 0.011 | 0.028 | 0.047 | 0.066 | 0.020 | 0.045 |
| MgO | 2.29 | 2.83 | 2.77 | 2.55 | 3.01 | 1.67 | 0.54 |
| CaO | 0.09 | 0.01 | 0.00 | 0.04 | 0.04 | 0.07 | 0.08 |
| Total | 97.83 | 98.03 | 97.33 | 96.45 | 97.49 | 95.82 | 96.08 |
| $Si^{4+}$ | 0.0047 | 0.0265 | 0.0026 | 0.0034 | 0.0033 | 0.0015 | 0.0022 |
| $Ti^{4+}$ | 0.0113 | 0.0130 | 0.0115 | 0.0116 | 0.0118 | 0.0250 | 0.0140 |
| $Al^{3+}$ | 0.5430 | 0.5570 | 0.5749 | 0.5496 | 0.5644 | 0.3815 | 0.6322 |
| $Cr^{3+}$ | 1.2858 | 1.2687 | 1.3062 | 1.3059 | 1.3069 | 1.3257 | 1.2357 |
| $Fe^{2+}$ | 0.8755 | 0.8531 | 0.8546 | 0.8623 | 0.8401 | 0.9059 | 0.9669 |
| $Fe^{3+}$ | 0.1551 | 0.1348 | 0.1047 | 0.1295 | 0.1137 | 0.2663 | 0.1159 |
| $Ni^{2+}$ | 0.0013 | 0.0003 | 0.0008 | 0.0013 | 0.0019 | 0.0006 | 0.0013 |
| $Mg^{2+}$ | 0.1197 | 0.1463 | 0.1446 | 0.1348 | 0.1566 | 0.0907 | 0.0288 |
| $Ca^{2+}$ | 0.0035 | 0.0003 | 0.0000 | 0.0016 | 0.0015 | 0.0027 | 0.0030 |
| Cr/(Cr + Al) | 0.703 | 0.695 | 0.694 | 0.704 | 0.698 | 0.777 | 0.662 |
| Mg/(Mg + Fe) | 0.120 | 0.146 | 0.145 | 0.135 | 0.157 | 0.091 | 0.029 |

**Table 4** Representative microprobe data for volcanic glass (*ND* not detected)

| Sample no. Location | 91105 Matrix | 91105 Matrix | 91105 Matrix | 91105 Hollow olivine | 91105 Matrix | 91118/1 Matrix | 91118/1 Matrix |
|---|---|---|---|---|---|---|---|
| $SiO_2$ | 49.25 | 51.59 | 49.64 | 53.16 | 51.66 | 55.16 | 51.89 |
| $TiO_2$ | 1.890 | 0.826 | 0.954 | 0.882 | 0.517 | 0.782 | 0.797 |
| $Al_2O_3$ | 16.98 | 17.08 | 15.70 | 17.97 | 18.32 | 20.24 | 18.18 |
| $Cr_2O_3$ | 0.02 | 0.04 | 0.05 | 0.02 | 0.02 | 0.02 | 0.03 |
| FeO | 11.12 | 9.02 | 11.71 | 9.60 | 9.21 | 5.34 | 10.07 |
| MnO | 0.456 | 0.200 | 0.243 | 0.204 | 0.150 | 0.090 | 0.068 |
| NiO | 0.032 | ND | ND | 0.011 | 0.043 | 0.015 | ND |
| MgO | 6.74 | 5.79 | 7.93 | 4.96 | 4.88 | 2.66 | 4.00 |
| CaO | 8.52 | 9.94 | 8.32 | 8.72 | 9.78 | 8.41 | 10.16 |
| $Na_2O$ | 3.49 | 3.68 | 2.80 | 4.03 | 4.10 | 5.40 | 3.05 |
| $K_2O$ | 0.11 | 0.24 | 1.10 | 0.18 | 0.11 | 0.05 | 0.18 |
| Total | 98.61 | 98.41 | 98.46 | 99.74 | 98.78 | 98.17 | 98.43 |

amygdules. It lies well above the olivine control lines and was excluded from the following discussion and petrologic modeling. Nickel shows a behavior similar to that of MgO, revealing a strong negative correlation with the above components ($r = 0.99$–$1.00$). When plotted against Ni, the olivine control lines give intercepts at $2410 \pm 70$ ppm ($2\sigma_{mean}$); this value corresponds to the average Ni content in the liquidus olivine (Table 1). Chromium is positively correlated with MgO, which suggests that along with olivine, chromite was a liquidus phase over the whole compositional range of the crystallization of the lake. The alkalis show either poor correlation with MgO ($r = 0.82$ for $Na_2O$), or mostly irregular behavior ($K_2O$, Rb), and are regarded as having been mobile during the low-grade metamorphism.

Ratios $CaO/Al_2O_3$ ($0.82 \pm 0.01$), $Al_2O_3/TiO_2$ ($19.6 \pm 0.3$), and Ti/Y ($249 \pm 4$, $2\sigma_{mean}$) are close to chondritic values of 0.80, 22, and 275, respectively (Hart and Zindler 1986; McDonough and Sun 1995) while Zr/Y ratios ($3.86 \pm 0.04$) are substantially higher, and Ti/Zr ($64.4 \pm 0.8$) lower than those in chondrites (2.5 and 110), implying significant enrichment of the rocks in Zr relative to Ti and Y.

Shown in Fig. 5 are patterns for selected major, trace and rare earth elements normalized to primitive mantle values of Hofmann (1988). The patterns are strongly parallel, with abundances reversely correlated with MgO content. In line with the enrichment in Zr, the rocks are also enriched in Sr, Ba, and LREE [chondrite normalized $(La/Sm)_N = 2.1$–$2.3$] and reveal strong negative Nb- and Ti-anomalies [$(Nb/Ba)_N = 0.12 \pm 0.01$, $(Nb/La)_N = 0.26 \pm 0.02$]. Europium shows slight negative anomalies ($Eu/Eu^* = 0.94$–$0.97$).

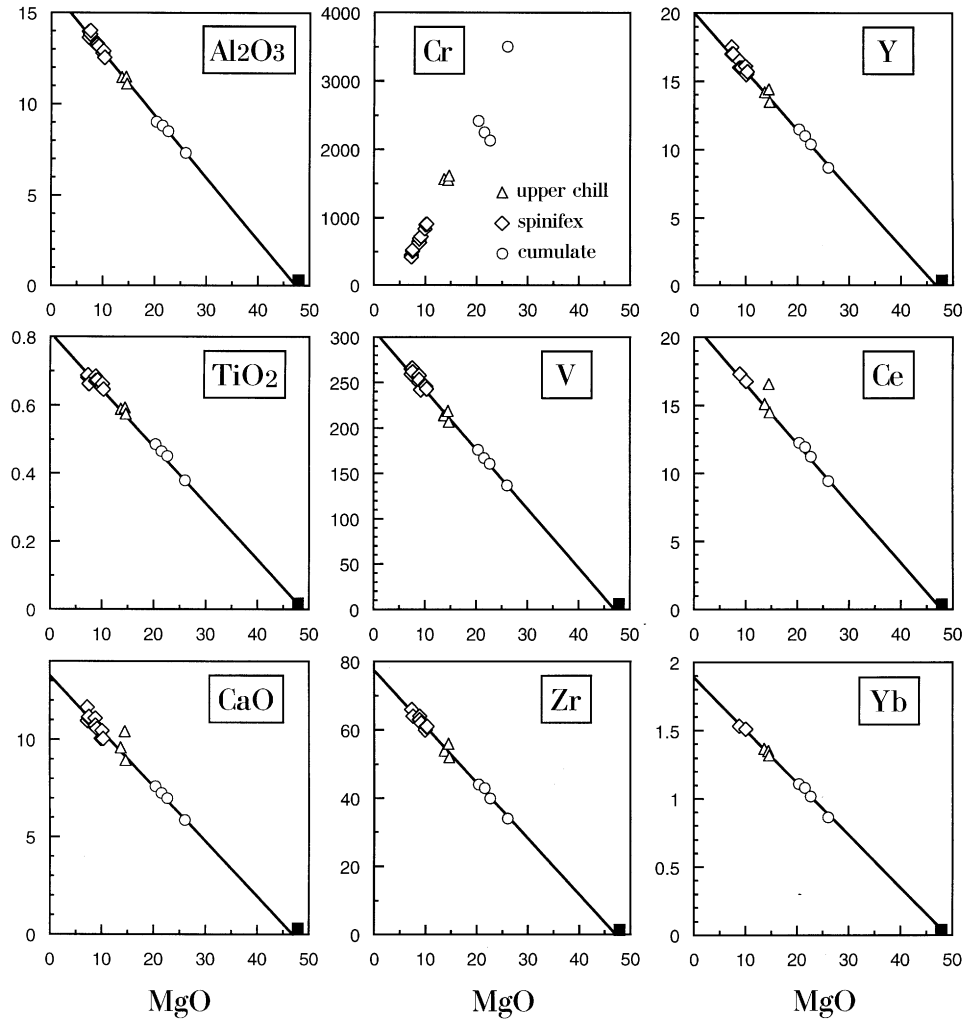


**Fig. 4** Variation diagrams of selected major and trace elements for Victoria's lava lake. The calculated and measured liquidus olivine composition is shown by *solid square*

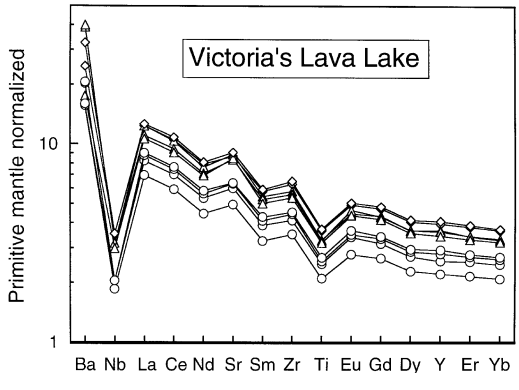


**Fig. 5** Abundances of selected major, trace and rare earth elements normalized to primitive mantle values of Hofmann (1988) in Victoria's lava lake. Legend same as in Fig. 4

## Sm–Nd isotope data

Sm–Nd isotope data are listed in Table 6 and plotted on the conventional Sm–Nd diagram (Fig. 6). Bulk rock samples representing the whole section through the lake from top to bottom as well as olivine, augite and pigeonite mineral separates define a well-constrained [mean standard weighted deviates MSWD = 1.1] isochron with a slope corresponding to an age of 2410 ± 34 Ma and a negative initial εNd(T) value of − 0.9 ± 0.2.

## Discussion

### Lake, flow or sill?

In this paper, the thick differentiated unit containing olivine cumulate layer was referred to as a lava lake. The most convincing evidence that it is an extrusive body and not a sill comes from such crucial indicators of volcanic nature as the asymmetric structure typical of komatiitic lavas (e.g., Arndt et al. 1977; Arndt 1986b; Renner et al. 1994) and the presence of the upper breccia, or scoria – a prominent rock consisting of vitreous blocky fragments of lava. In contrast to polygonal jointing, these fragments show displacement

**Table 5** Major, trace and rare earth element data for Victoria's lava lake.The analyses are normalized to 100% on an anhydrous basis (*LOI* loss on ignition).

| Sample no. | 91100 | 91101 | 91102 | 91103 | 91104 | 91105 | 91106 | 91107 | 91108 | 91109 | 91110 | 91112 | 91113 |
|---|---|---|---|---|---|---|---|---|---|---|---|---|---|
| SiO2 | 51.6 | 52.4 | 51.7 | 48.2 | 47.9 | 46.0 | 47.8 | 52.9 | 52.6 | 52.1 | 50.3 | 50.5 | 49.3 |
| $TiO_2$ | 0.646 | 0.672 | 0.670 | 0.485 | 0.464 | 0.379 | 0.451 | 0.662 | 0.662 | 0.681 | 0.575 | 0.589 | 0.593 |
| $Al_2O_3$ | 12.5 | 13.2 | 13.3 | 9.0 | 8.8 | 7.3 | 8.5 | 13.8 | 14.0 | 14.0 | 11.1 | 11.5 | 11.5 |
| $Fe_2O_3$ | 11.5 | 11.1 | 11.0 | 11.9 | 11.7 | 12.3 | 11.7 | 10.6 | 10.6 | 11.2 | 12.1 | 11.6 | 11.3 |
| MnO | 0.194 | 0.191 | 0.193 | 0.170 | 0.182 | 0.185 | 0.177 | 0.183 | 0.194 | 0.204 | 0.185 | 0.173 | 0.184 |
| MgO | 10.3 | 8.85 | 8.85 | 20.4 | 21.6 | 26.1 | 22.6 | 7.54 | 7.55 | 7.29 | 14.6 | 13.7 | 14.5 |
| CaO | 10.0 | 10.7 | 10.6 | 7.62 | 7.26 | 5.88 | 7.00 | 11.1 | 11.2 | 11.7 | 8.96 | 9.59 | 10.4 |
| $Na_2O$ | 2.90 | 2.21 | 3.07 | 1.89 | 1.68 | 1.62 | 1.28 | 2.79 | 2.73 | 2.67 | 1.63 | 2.03 | 1.90 |
| $K_2O$ | 0.17 | 0.47 | 0.48 | 0.26 | 0.32 | 0.22 | 0.39 | 0.29 | 0.35 | 0.20 | 0.43 | 0.35 | 0.26 |
| $P_2O_5$ | 0.08 | 0.09 | 0.09 | 0.08 | 0.07 | 0.06 | 0.07 | 0.11 | 0.11 | 0.11 | 0.08 | 0.09 | 0.09 |
| LOI | 0.70 | 0.19 | 0.17 | 1.22 | 0.69 | 2.04 | 0.89 | 0.22 | 0.25 | 0.16 | 2.50 | 1.50 | 2.42 |
| Cr | 909 | 688 | 628 | 2417 | 2255 | 3507 | 2131 | 502 | 525 | 447 | 1619 | 1570 | 1552 |
| V | 243 | 253 | 258 | 176 | 167 | 137 | 161 | 266 | 262 | 265 | 207 | 214 | 219 |
| Co | 45 | 47 | 39 | 87 | 91 | 107 | 96 | 35 | 39 | 34 | 67 | 56 | 58 |
| Ni | 216 | 119 | 106 | 801 | 874 | 1138 | 952 | 68 | 70 | 61 | 408 | 348 | 386 |
| Zr | 61 | 63 | 64 | 44 | 43 | 34 | 40 | 64 | 64 | 66 | 52 | 54 | 56 |
| Nb | 2.2 | 2.2 | 2.2 | 1.3 | 1.3 | 1.1 | 1.3 | 2.6 | 2.6 | 2.6 | 1.8 | 2.0 | 2.0 |
| Y | 15.7 | 16 | 16 | 11.5 | 11 | 8.7 | 10.1 | 17 | 17 | 17.5 | 13.5 | 14.2 | 14.4 |
| Sr | 164 | 165 | 172 | 116 | 115 | 90 | 109 | 164 | 175 | 176 | 154 | 152 | 161 |
| Rb | 5 | 8 | 7 | 5 | 7 | 4 | 9 | 6 | 7 | 4 | 10 | 9 | 5 |
| Ba | 190 | 197 | 180 | 97 | 125 | 95 | 123 | 180 | 184 | 190 | 106 | 242 | 236 |
| La | | 7.75 | | 5.54 | 5.38 | 4.27 | 5.05 | | | | 6.52 | 6.78 | 7.60 |
| Ce | | 17.3 | | 12.3 | 11.9 | 9.5 | 11.2 | | | | 14.5 | 15.1 | 16.6 |
| Nd | | 9.63 | | 6.91 | 6.68 | 5.30 | 6.34 | | | | 8.24 | 8.45 | 9.09 |
| Sm | | 2.28 | | 1.65 | 1.59 | 1.26 | 1.50 | | | | 1.94 | 2.03 | 2.10 |
| Eu | | 0.734 | | 0.533 | 0.508 | 0.404 | 0.494 | | | | 0.634 | 0.672 | 0.646 |
| Gd | | 2.47 | | 1.75 | 1.71 | 1.36 | 1.61 | | | | 2.13 | 2.19 | 2.21 |
| Dy | | 2.63 | | 1.88 | 1.83 | 1.46 | 1.73 | | | | 2.26 | 2.34 | 2.32 |
| Er | | 1.62 | | 1.15 | 1.12 | 0.896 | 1.06 | | | | 1.37 | 1.42 | 1.42 |
| Yb | | 1.53 | | 1.11 | 1.08 | 0.865 | 1.02 | | | | 1.32 | 1.37 | 1.35 |
| Mg/(Mg + Fe) | 0.639 | 0.612 | 0.614 | 0.773 | 0.785 | 0.808 | 0.793 | 0.584 | 0.585 | 0.564 | 0.706 | 0.700 | 0.717 |
| Ti/Zr | 63.5 | 64.0 | 62.8 | 66.1 | 64.7 | 66.9 | 67.5 | 62.0 | 62.0 | 61.8 | 66.3 | 65.4 | 63.5 |
| Zr/Y | 3.89 | 3.94 | 4.00 | 3.83 | 3.91 | 3.91 | 3.96 | 3.76 | 3.76 | 3.77 | 3.85 | 3.80 | 3.89 |
| $(La/Nb)_N$ | | 3.6 | | 4.4 | 4.3 | 3.7 | 4.0 | | | | 3.6 | 3.5 | 3.9 |
| $(La/Sm)_N$ | | 2.14 | | 2.11 | 2.13 | 2.14 | 2.12 | | | | 2.12 | 2.10 | 2.28 |
| $(Gd/Yb)_N$ | | 1.30 | | 1.27 | 1.27 | 1.27 | 1.28 | | | | 1.30 | 1.30 | 1.32 |
| Eu/Eu* | | 0.945 | | 0.957 | 0.943 | 0.946 | 0.971 | | | | 0.954 | 0.974 | 0.917 |

**Table 6** Nd-isotopic data for Victoria's lava lake (*WR* bulk rock samples, *OI* olivine, *Aug* augite, *Pig* pigeonite mineral separates respectively)

| Sample no. | Sm, ppm | Nd, ppm | $^{147}Sm/^{144}Nd$ | $^{143}Nd/^{144}Nd$ | εNd(2410) |
|---|---|---|---|---|---|
| 91103 WR | 1.631 | 6.923 | 0.14238 | $0.511739 \pm 8$ | − 0.71 |
| 91103 Aug | 1.325 | 3.724 | 0.21508 | $0.512884 \pm 8$ | − 0.90 |
| 91103 Ol | 0.1738 | 0.625 | 0.16819 | $0.512156 \pm 9$ | − 0.57 |
| 91104 WR | 1.603 | 6.808 | 0.14233 | $0.511710 \pm 7$ | − 1.3 |
| 91104 Aug | 1.397 | 3.976 | 0.21238 | $0.512826 \pm 7$ | − 1.2 |
| 91104 Pig | 0.563 | 1.917 | 0.17751 | $0.512284 \pm 9$ | − 0.97 |
| 91106 WR | 1.522 | 6.381 | 0.14420 | $0.511751 \pm 7$ | − 1.0 |
| 91106 Aug | 1.265 | 3.699 | 0.20681 | $0.512753 \pm 8$ | − 0.90 |
| 91106 Ol | 0.0492 | 0.168 | 0.17708 | $0.512291 \pm 11$ | − 0.69 |
| 91101 WR | 2.306 | 9.731 | 0.14322 | $0.511737 \pm 7$ | − 1.0 |
| 91105 WR | 1.248 | 5.209 | 0.14475 | $0.511764 \pm 4$ | − 0.96 |
| 91117 WR | 2.255 | 9.516 | 0.14324 | $0.511743 \pm 8$ | − 0.90 |

relative one another, i.e., it is a true breccia. The fragments are interpreted to have been detached from the continuously solidifying foundered roof and incorporated within the upper part of flowing lava. Both ancient lava lakes and their modern equivalents were shown to contain scorias (Arndt 1986c; Wright et al. 1968; Helz et al. 1989). We interpret this volcanic unit as a lava lake owing to its large thickness and high-Mg composition. High-magnesian liquids have a very low viscosity (Arndt 1976; Huppert et al. 1984), which prevents them

| 91117 | 91119 | 91121 | 91122 | 91124 |
|---|---|---|---|---|
| 51.3 | 51.2 | 51.4 | 51.5 | 52.5 |
| 0.662 | 0.651 | 0.684 | 0.673 | 0.688 |
| 12.9 | 12.8 | 13.2 | 13.2 | 13.6 |
| 11.7 | 11.5 | 11.6 | 11.4 | 11.0 |
| 0.201 | 0.204 | 0.194 | 0.205 | 0.203 |
| 10.1 | 9.94 | 8.81 | 9.16 | 7.30 |
| 10.4 | 10.0 | 11.1 | 10.6 | 11.0 |
| 2.52 | 3.41 | 2.36 | 2.81 | 3.14 |
| 0.13 | 0.19 | 0.52 | 0.45 | 0.53 |
| 0.09 | 0.09 | 0.12 | 0.10 | 0.09 |
| 0.18 | 0.32 | 0.40 | 0.39 | 0.21 |
| 898 | 837 | 653 | 721 | 417 |
| 246 | 247 | 250 | 242 | 259 |
| 53 | 55 | 52 | 53 | 42 |
| 174 | 193 | 112 | 122 | 54 |
| 61 | 60 | 63 | 62 | 66 |
| 2.2 | 2.2 | 2.2 | 2.2 | 2.2 |
| 15.5 | 16.1 | 16.5 | 16 | 17 |
| 158 | 172 | 171 | 166 | 169 |
| 3 | 5 | 5 | 5 | 8 |
| 150 | 160 | 205 | 187 | 190 |
| 7.59 | | | | |
| 16.8 | | | | |
| 9.43 | | | | |
| 2.23 | | | | |
| 0.716 | | | | |
| 2.41 | | | | |
| 2.58 | | | | |
| 1.58 | | | | |
| 1.51 | | | | |
| 0.632 | 0.632 | 0.601 | 0.613 | 0.568 |
| 65.1 | 65.1 | 65.1 | 65.0 | 62.5 |
| 3.94 | 3.73 | 3.82 | 3.88 | 3.88 |
| 3.5 | | | | |
| 2.14 | | | | |
| 1.29 | | | | |
| 0.943 | | | | |

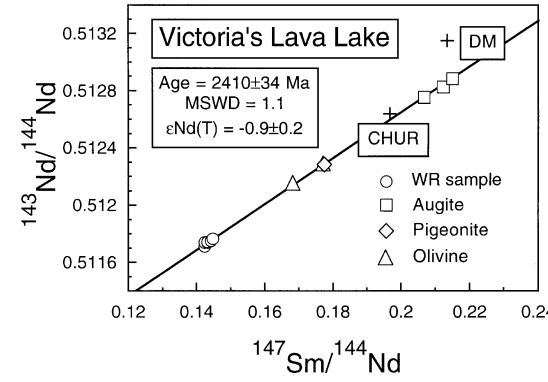


**Fig. 6** Conventional Sm-Nd diagram for Victoria's lava lake. The present-day parameters of the chondrite uniform reservoir (*CHUR*) were adopted from Jacobsen and Wasserburg (1980, 1984) to be the following: $^{147}Sm/^{144}Nd = 0.1967$, $^{143}Nd/^{144}Nd = 0.512638$. The parameters of the model depleted mantle reservoir (*DM*) are $^{147}Sm/^{144}Nd = 0.2135$, $^{143}Nd/^{144}Nd = 0.513151$ and correspond to the $\varepsilon Nd_{(DM)}(T = 0) = +10$ and the time of fractionation from CHUR 4.6 Ga ago

from forming thick continuous lava bodies unless they are ponded. As can be seen in Fig. 1, the studied unit represents an unusually thick body in this area, which probably formed under uniquely favorable conditions. These conditions were obviously not met for the other lava units, which are much thinner and virtually undifferentiated. Field relations suggest that the lake is getting thicker to the west and is gradually pinching out to the east. It might well have been that its shape was controlled by a large topographic low or a previously formed trough-like structure.

## Composition and evolution of the erupted liquid

According to the petrographic observations, the only minerals present as phenocrysts or cumulus phases are olivine and chromite. It is very likely therefore, that the evolution of the primary magma after eruption was controlled by fractionation of these minerals only. This conclusion is also supported by the analysis of the variation diagrams, in which all elements but Ni and Cr are reversely correlated with MgO.

In order to deduce the liquid compositions, several independent approaches were used. The amygdule-free chilled sample 91110, containing 14.7% MgO, is essentially a glassy rock, consisting of phenocrysts in a quenched groundmass. Obviously, it did not undergo any post-eruption differentiation and is interpreted to have a bulk composition very similar to that of the liquid from which it has formed. The second approach to estimate the composition of the primary lava was to calculate the liquid compositions using olivine data. The most magnesian olivines ($Fo_{88.7-88.9}$) were documented in the upper and lower chilled margins of the lake. If a $K_{D(ol-liq)}^{Mg-Fe} = 0.31$ (Beattie et al. 1991) is adopted, then, taking into account the Mg/Fe relationships in the studied komatiitic basalts, these olivines can be shown to have been in equilibrium with a liquid containing 14.8–15.2% MgO. The liquid and equilibrium olivine compositions can also be inferred using an indirect approach based on the general differentiation trends established for the lava lake. In the plots MgO versus an element that is excluded from the olivine crystal lattice [$K_{D(ol-liq)} \ll 1$], the analytical data for samples containing different proportions of olivine crystallized from a common parental melt fall on the mixing lines (olivine control lines). The intercept of these regression lines with the MgO axis corresponds directly to the average composition of liquidus olivine. For the studied suite of samples, this value is equal to $47.9 \pm 0.7\%$ MgO. Recalculating for the olivine stoichiometry, this gives an olivine composition of $Fo_{88.7}$, in excellent agreement with the results of the olivine microprobe studies. Thus three independent

lines of evidence indicate that komatiitic basalts from the Lion Hills area erupted with liquid compositions of $\sim 15\%$ MgO.

## Eruption temperature, thermal history and internal differentiation of the lava lake

In order to calculate the eruption temperature of the komatiitic basalt melt, the procedures described by Abbott et al. (1994) and Nisbet et al. (1993) are particularly suitable. The chemical analyses of the upper chilled margin were used to calculate the eruption temperature on the basis of the well-known assumption that the Fe/Mg ratio in a primitive magma is directly related to its liquidus temperature (Roeder and Emslie 1970; Hanson and Langmuir 1978). Calculations show that the komatiitic basalt magma erupted onto the surface with liquidus temperatures of 1380–1400 °C (Table 7). The liquidus temperatures for the samples from the spinifex zone vary from 1320–1310 °C for the plate olivine spinifex layer to 1310–1280 °C for the pyroxene spinifex and to 1250 °C for the fine-grained basalt layer. In order to obtain an estimate for the solidus temperatures of crystallization of the lava lake, we applied the above procedure to the analyses of the fresh volcanic glass (Table 4), which represents the last portions of the trapped liquid. Calculated temperatures vary over a wide range between 1270–1070 °C depending on the composition of the glass. The crystallization interval for the lake is therefore estimated to be between 1400–1070 °C.

The main liquidus phases in the lava lake are olivine and chromite. The partitioning of Fe and Mg between these two minerals also can be utilized to estimate the eruption temperature of the magmas. We used Lehmann's equation to calculate the liquidus temperatures (Lehmann 1983). In order to avoid disequilibrium bias, we studied only intergrown or adjacent olivine and chromite grains. All studied samples come from the cumulate zone. The temperatures obtained range from 970 to 1040 °C (Table 8) and are hence lower than those calculated from the MgO content in the primary liquid or inferred from the experimental studies (Arndt 1976; Thy 1995), while being similar to crystallization temperatures for the last and most evolved portions of the trapped liquid.

The temperature estimates based on the two-pyroxene thermometer are listed in Table 8. The selected samples come from the basal chilled margin and the middle part of the spinifex zone, where skeletal augite and pigeonite grains are found to occur in close spatial association. The estimated temperatures range from 1185 to 1225 °C using the thermometer of Lindsley (1983). These temperatues are slightly lower than the liquidus temperatures of the pyroxene spinifex-textured rocks, but agree well with the experimental results of Kinzler and Grove (1985) and Thy (1995) and are interpreted to correspond to the crystallization temperatures of the augite-pigeonite pairs.

From the field relationships and the petrographic observations it can be concluded that a magnesian (15% MgO) komatiitic basalt liquid, containing 15 to 20% olivine phenocrysts during the eruption filled a large deep topographic depression, located distinctly to the side of the main lava channel. As a result, a large volume of magma ponded and stopped flowing. This in turn allowed efficient olivine settling to form the layered structure of the lake. Judging from the continuous, undisturbed structure of the lake, it was probably filled to its present depth in a large single pulse or several smaller but almost contemporaneous pulses of magma. Many of the polyhedral olivine grains in the lava lake are regarded as being transported by the lava as phenocrysts and crystallized before emplacement. Only a smaller part of the whole population, mostly hopper crystals and overgrowths on the polyhedral grains, were formed *in situ*. This is suggested by the uniform and close compositions of phenocryst cores both in the upper chilled margin and cumulate zone, implying their slow equilibrium crystallization from a large volume of a magma prior to eruption.

After phenocrysts were removed from the part of the lake immediately below the upper chilled margin, the spinifex zone started to form proceeding from the top downward. The wide textural and mineralogical variability of this zone at largely constant chemical composition is attributed mainly to a different degree of supercooling attained in each successive layer in the crystallizing liquid, and to its boundary composition (from 10 to 9% MgO), at which olivine is replaced by clinopyroxene on the liquidus (Arndt 1976). The reverse sequence of crystallization, when clinopyroxene is replaced by olivine on the liquidus, as evidenced by the intercalation of olivine and pyroxene spinifex layers, can be explained by temperature increase at the front of crystallization caused by the heat released during very fast spinifex pyroxene nucleation. Besides,

**Table 7** Results of liquidus temperatures calculations for Victoria's lava lake

| | | | | | | | |
|---|---|---|---|---|---|---|---|
| Sample | 91110 | 91112 | 91113 | 91100 | 91101 | 91102 | 91107 |
| Tliq(°C) | 1398 | 1381 | 1393 | 1317 | 1280 | 1287 | 1247 |
| Sample | 91108 | 91109 | 91117 | 91119 | 91121 | 91122 | 91124 |
| Tliq(°C) | 1248 | 1239 | 1309 | 1313 | 1282 | 1293 | 1247 |
| Sample | Glass 1 | Glass 2 | Glass 3 | Glass 4 | Glass 5 | Glass 6 | Glass 7 |
| Tliq(°C) | 1230 | 1200 | 1274 | 1170 | 1168 | 1068 | 1127 |

**Table 8** Calculated temperatures from olivine-chromite and augite-pigeonite pairs

| Sample | 91105 (1) | 91105 (2) | 91105 (3) | 91105 (4) | 91105 (5) |
|---|---|---|---|---|---|
| | | | Chromite | | |
| $Al^{3+}$ | 0.5430 | 0.5570 | 0.5749 | 0.5496 | 0.5644 |
| $Cr^{3+}$ | 1.2858 | 1.2687 | 1.3062 | 1.3059 | 1.3069 |
| $Fe^{2+}$ | 0.8755 | 0.8531 | 0.8546 | 0.8623 | 0.8401 |
| $Fe^{3+}$ | 0.1551 | 0.1348 | 0.1047 | 0.1295 | 0.1137 |
| $Mg^{2+}$ | 0.1197 | 0.1463 | 0.1446 | 0.1348 | 0.1566 |
| | | | Olivine | | |
| $Fe^{2+}$ | 0.2606 | 0.2937 | 0.2852 | 0.303 | 0.2895 |
| $Mg^{2+}$ | 1.7233 | 1.6915 | 1.699 | 1.6808 | 1.6939 |
| $T$(°C) | 969 | 1038 | 1018 | 1025 | 1035 |

| Sample | 91104 (1) | 91104 (2) | 91106 (1) | 91106 (2) | 91117 |
|---|---|---|---|---|---|
| | | | Augite | | |
| $Si^{4+}$ | 1.9251 | 1.9192 | 1.9062 | 1.9061 | 1.9330 |
| $Ti^{4+}$ | 0.0130 | 0.0177 | 0.0212 | 0.0153 | 0.0096 |
| $Al^{IV}$ | 0.0749 | 0.0808 | 0.0832 | 0.0835 | 0.0670 |
| $Al^{VI}$ | 0.0336 | 0.0136 | 0.0000 | 0.0000 | 0.0853 |
| $Cr^{3+}$ | 0.0118 | 0.0127 | 0.0032 | 0.0104 | 0.0088 |
| $Fe^{3+}$ | 0.0149 | 0.0348 | 0.0657 | 0.0664 | 0.0000 |
| $Fe^{2+}$ | 0.1823 | 0.2093 | 0.2105 | 0.2129 | 0.2452 |
| $Mn^{2+}$ | 0.0053 | 0.0056 | 0.0061 | 0.0079 | 0.0063 |
| $Mg^{2+}$ | 0.9270 | 0.9510 | 0.9616 | 1.0113 | 0.9861 |
| $Ca^{2+}$ | 0.8005 | 0.7382 | 0.7227 | 0.6716 | 0.6742 |
| $Na^{+}$ | 0.0114 | 0.0158 | 0.0175 | 0.0135 | 0.0151 |
| | | | Pigeonite | | |
| $Si^{4+}$ | 1.9763 | 1.9620 | 1.9493 | 1.9505 | 1.9613 |
| $Ti^{4+}$ | 0.0087 | 0.0064 | 0.0090 | 0.0066 | 0.0031 |
| $Al^{IV}$ | 0.0237 | 0.0380 | 0.0507 | 0.0490 | 0.0387 |
| $Al^{VI}$ | 0.0348 | 0.0175 | 0.0028 | 0.0000 | 0.0349 |
| $Cr^{3+}$ | 0.0091 | 0.0072 | 0.0061 | 0.0037 | 0.0131 |
| $Fe^{3+}$ | 0.0000 | 0.0022 | 0.0289 | 0.0377 | 0.0000 |
| $Fe^{2+}$ | 0.3950 | 0.3651 | 0.3355 | 0.4028 | 0.2836 |
| $Mn^{2+}$ | 0.0091 | 0.0096 | 0.0109 | 0.0099 | 0.0063 |
| $Mg^{2+}$ | 1.2737 | 1.3776 | 1.3194 | 1.3715 | 1.5100 |
| $Ca^{2+}$ | 0.2984 | 0.2115 | 0.2806 | 0.1604 | 0.1577 |
| $Na^{+}$ | 0.0036 | 0.0016 | 0.0051 | 0.0050 | 0.0028 |
| $T$(°C) | 1185 | 1200 | 1215 | 1230 | 1225 |

unstable pyroxene crystallization could also occur from a liquid with $> 9\%$ MgO owing to the high degrees of supercooling attained (Arndt and Fleet 1979; Campbell and Arndt 1982). The fine-grained basalt layer immediately overlying the cumulate zone and having a remarkably uniform composition represents the residual liquid and crystallized at the final stages of formation of the lava lake as indicated by the lowest liquidus temperatures (1240–1250 °C) and MgO content (7.3%) obtained for this layer. This layer is similar to the lowermost part of spinifex-textured zones in more magnesian komatiite lavas elsewhere (e.g., Arndt 1986b; Renner et al. 1994)

The observed mineral morphology and temperature estimates can be used to place some constraints on the thermal history of the lava lake. As shown by experimental data of Lofgren et al. (1974) and Donaldson (1976; 1982), the change in shape of olivine and pyroxene crystals as a function of cooling rate and degree of supercooling is systematic and common to all melts investigated. From our study of crystal morphology in the lava lake it can be inferred that the cooling rates and the degree of supercooling were highly variable, from 40–80 °C/h ($\Delta T = 50$–80 °C) in the spinifex zone to 1.2–15 °C/h ($\Delta T = 0$–30 °C) in the cumulate zone. It is apparent, however, that the cooling rates became much slower after a large proportion of cumulus olivine had settled and the grains thus formed a self-supporting framework. Convection of the liquid was then mostly inhibited and cooling proceeded dominantly by means of conduction.

Turner et al. (1986) and Gole et al. (1990) noted that the center of thick extrusive bodies remains at a temperature close to the liquidus for some tens of years depending on their thickness, while the top cools rapidly to the ambient surface temperature. These conclusions

are also supported by direct cooling rate measurements from the Kilauea Iki lava lake, Hawaii (Helz et al. 1989). This lava lake formed in 1959 as a large pond of picritic basalt (15% MgO) and has cooled and crystallized as a self-roofed magma chamber approximately 115 meters deep. All processes of large-scale internal differentiation occurring in the lake ceased sometime between 1979 and 1981. If the crystallization time interval for Victoria's lava lake, which has about the same depth and primary liquid composition, was of the same order of magnitude, it becomes clear that the central part of the body cooled very slowly. Therefore it is not unexpected that cation exchange in the olivine-spinel pairs ceased late and this system was finally frozen at nearly solidus temperatures.

## Sm–Nd isotope data and the age of the lava lake

The Sm–Nd isochron age of 2410 $\pm$ 34 Ma represents a reliable estimate of the crystallization age of the lava lake in particular and, more generally, the timing of accumulation of the Vetreny Belt suite. This in turn provides an estimate for the final stages of magmatism in the Vetreny Belt. The whole rock samples reveal a very narrow range in Nd-isotope compositions and Sm/Nd ratios throughout the lava lake, implying that the erupted melt was chemically very homogeneous and no contamination occurred after emplacement of the lava onto the surface. Within analytical uncertainty, this age is in good agreement with the Sm-Nd and Pb-Pb isochron ages of 2449 $\pm$ 35 and 2424 $\pm$ 178 Ma, respectively, obtained for volcanic rocks from the same suite in Golets Hills, northwestern Vetreny Belt (Puchtel et al. 1991).

As can be seen in Table 6, the olivine, pigeonite and augite separates are characterized by relatively high Nd and Sm concentrations. Assuming that abundances of these elements in sample 91110 correspond to those in the erupted melt, it is possible to calculate theoretical contents of these elements in the studied olivine and low- and high-Ca pyroxenes using published partition coefficients. As can be seen from Table 9, the measured values for olivine are 30–250 times, for pigeonite 8–15 times, and for augite 1.5–3 times higher than the theoretical abundances. These discrepancies are likely to be ascribed to the presence of tiny glass inclusions in the mineral separates, mostly inside hopper crystals. Calculations show that some 1–2% of these inclusions would be enough to account for all the excess Nd. Although these inclusions cannot shift the isotope equilibrium between the crystals and the liquid, and, therefore, do not alter the interpretation of the isochron, they have substantial effect on the Sm/Nd ratio in the mineral separates. As seen in Table 9, the measured $^{147}Sm/^{144}Nd$ in the olivine is 2.5 times, in the pigeonite – almost 2 times, and in augite – 7–30% lower than the calculated values.

## Composition of parental magmas and isotope characteristics of the mantle source region

Despite the obvious compositional differences between the continental crust and mantle, the effect of crustal contamination is not so easily recognizable. This is ascribed to the fact that, at least in some instances, the influence of crustal contamination is almost indistinguishable from the geochemical effects on basaltic magmas derived from a depleted asthenospheric source and then mixed with a component of the ancient continental lithosphere (Glazner and Farmer 1992; Brandon et al. 1993). Ryabchikov et al. (1988) suggested that komatiitic basalt magmas of the Vetreny Belt were

**Table 9** Comparison of calculated and measured Nd and Sm concentrations in mineral separates

| Mineral separate | Nd, ppm | Sm, ppm | $^{147}Sm/^{144}Nd$ | Reference |
|---|---|---|---|---|
| | | Partition coeffcicents used | | |
| Olivine | 0.0003 | 0.0009 | | Green 1994 |
| Low-Ca Pyroxene | 0.015 | 0.035 | | Green 1994 |
| Ca-Pyroxene | 0.15 | 0.30 | | Green 1994 |
| | 0.19 | 0.30 | | Hart and Dunn 1993 |
| | 0.30 | 0.54 | | Mc Rae and Russel 1987 |
| | | Concentrations and ratios calculated (1) and measured (2) | | |
| Melt (2) | 8.24 | 1.94 | 0.142 | |
| Olivine (1) | 0.0025 | 0.0017 | 0.411 | Green 1994 |
| 91103 Olivine (2) | 0.625 | 0.174 | 0.168 | |
| 91106 Olivine (2) | 0.168 | 0.0492 | 0.177 | |
| Low-Ca Pyroxene (1) | 0.124 | 0.0679 | 0.332 | Green 1994 |
| 91104 Pigeonite (2) | 1.92 | 0.563 | 0.178 | |
| Ca-Pyroxene (1) | 1.24 | 0.582 | 0.284 | Green 1994 |
| | 1.57 | 0.582 | 0.224 | Hart and Dunn 1993 |
| | 2.47 | 1.05 | 0.256 | Mc Rae and Russel 1987 |
| 91103 Augite (2) | 3.72 | 1.33 | 0.215 | |
| 91104 Augite (2) | 3.98 | 1.40 | 0.212 | |
| 91106 Augite (2) | 3.70 | 1.27 | 0.207 | |

derived from the enriched continental lithospheric mantle because of the apparent large-scale homogeneity of the lavas. Our more extensive studies indicate however that these lavas are very variable in terms of trace element and isotope characteristics (Puchtel IS, Haase KM, Hofmann AW, Chauvel C, Kulikov VS, Garbe-Schönberg D, submitted). We argue that the evolution of magmas parental to the Vetreny Belt komatiitic basalts was mainly controlled by assimilation of crustal rocks *en route* to the surface.

Due to very high liquidus temperatures and low viscosities, komatiitic melts are very susceptible to contamination by crustal rocks (e.g., Arndt 1986a; Arndt and Jenner 1986; Cattell 1987; Lesher and Arndt 1995). Contamination normally occurs during ascent or eruption (Huppert et al. 1984; Huppert and Sparks 1985) and results in a sharp increase in abundances of the elements concentrated in the upper continental crust, e.g., Ba, Zr, and LREE, in primary asthenospheric melts, but will have little effect on the concentrations of elements Ti, Nb and HREE. On average, this causes the origin of negative Nb- and Ti-anomalies in crustally contaminated rocks (Jochum et al. 1991). In contrast, the subcontinental mantle lithosphere is enriched in Nb relative to La (McDonough 1990). The studied volcanic rocks exhibit pronounced negative Nb- and Ti-anomalies relative to neighboring elements with a comparable degree of incompatibility, i.e., La, Ba and Zr $[(Nb/Ba)_N = 0.12 \pm 0.01, (Nb/La)_N = 0.26 \pm 0.02, (Ti/Zr)_N = 0.59 \pm 0.01, 2\sigma_{mean}]$. These relationships are most consistent with contamination of parental depleted komatiite magma with felsic material of the upper continental crust.

The upper crust in the Vodla and Belomorian Blocks consists of TTG-gneisses and amphibolites metamorphosed under amphibolite to granulite facies conditions and have ages of 3.1–3.2 and 2.7–2.8 Ga, respectively (Kulikov et al. 1990; Lobach-Zhuchenko et al. 1993; Bogdanova and Bibikova 1993; Timmerman and Daly 1995; Bibikova et al. in press). Trace element concentrations for these rocks, however, are not available and in order to prove or reject the assimilation hypothesis and to estimate the extent of contamination of the initial magma, the trace element composition of the bulk felsic Archean granulite reported by Rudnick and Fountain (1995) were used. The composition of this bulk analysis provides the closest approximation to the average composition of the upper crustal rocks in the Vodla and Belomorian Blocks area in terms of major elements. The average Nd-isotopic composition for these rocks ($^{143}Nd/^{144}Nd = 0.510746$) was adopted from the data of Kulikov et al. (1990), Lobach-Zhuchenko et al. (1993), Timmerman and Daly (1995), and Bibikova et al. (in press). As a possible equivalent to the primitive melt giving rise to the Lion Hills lavas, the composition of the 2.7 Ga old komatiite from the Belingwe greenstone belt (Nisbet et al. 1987; Jochum et al. 1991; Arndt et al. 1993) was chosen. This komatiite has 17.6% MgO, $^{143}Nd/^{144}Nd = 0.513197$, $\varepsilon Nd(T) = +2.5$, $(La/Sm)_N = 0.8$ and was suggested to have the composition close to that of the primary magma for the Vetreny Belt lavas based on major, trace element and olivine data (Puchtel IS, Haase KM, Hofmann AW, Chauvel C, Kulikov VS, Garbe-Schönberg D, submitted).

The results of the calculations are shown in Fig. 7. We used the ratios of selected elements, which are insensitive to fractional crystallization but are crucial indicators of assimilation processes. As can be seen in the diagrams Fig. 7, the erupted magma could have been derived from mixing of such an incompatible element depleted komatiite melt with upper crustal rocks. The inferred degrees of contamination are very consistent for different elemental ratios and vary slightly between 7 and 9%. Such contamination would have had only little effect on the major element composition of the initial magma (Table 9). The negative Eu-anomalies observed in the rocks were also shown to have been the results of crustal contamination. Based on these data therefore, little can be deduced with respect to the Nd-isotope composition of the mantle source region of the komatiitic basalts from the lava lake.

## Concluding remarks

1. Remarkably fresh by early Precambrian standards, komatiitic basalts from the uppermost part of the Vetreny Belt provide a sound source of information on the

**Table 10** Results of mixing calculations for major elements. Numbers correspond to percentage contamination. [*BK* Belingwe komatiite (Nisbet et al. 1987; Jochum et al. 1991), *UCC* felsic upper continental crust after Rudnick and Fountain (1995)]

| | BK | 2% | 4% | 6% | 8% | 10% | 20% | 30% | 40% | UCC |
|---|---|---|---|---|---|---|---|---|---|---|
| $SiO_2$ | 49.65 | 50.07 | 50.48 | 50.90 | 51.32 | 51.74 | 53.82 | 55.91 | 57.99 | 70.50 |
| $TiO_2$ | 0.430 | 0.429 | 0.429 | 0.428 | 0.428 | 0.427 | 0.424 | 0.421 | 0.418 | 0.400 |
| $Al_2O_3$ | 9.01 | 9.12 | 9.23 | 9.33 | 9.44 | 9.55 | 10.09 | 10.63 | 11.17 | 14.40 |
| FeO | 11.74 | 11.57 | 11.39 | 11.22 | 11.05 | 10.88 | 10.01 | 9.15 | 8.28 | 3.10 |
| MgO | 17.59 | 17.26 | 16.93 | 16.60 | 16.27 | 15.94 | 14.29 | 12.64 | 10.99 | 1.10 |
| CaO | 8.79 | 8.67 | 8.55 | 8.43 | 8.31 | 8.19 | 7.59 | 6.99 | 6.39 | 2.80 |
| $CaO/Al_2O_3$ | 0.976 | 0.951 | 0.927 | 0.903 | 0.880 | 0.858 | 0.753 | 0.658 | 0.573 | 0.194 |
| $Al_2O_3/TiO_2$ | 20.95 | 21.23 | 21.51 | 21.80 | 22.08 | 22.36 | 23.79 | 25.24 | 26.71 | 36.00 |

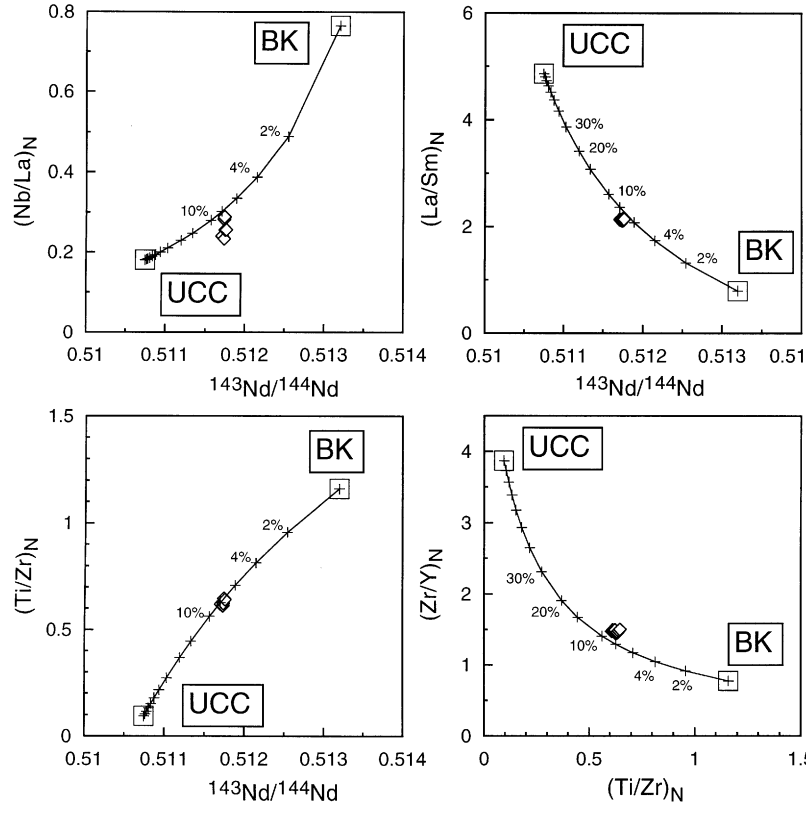


**Fig. 7** Diagrams $(Nb/La)_N$, $(La/Sm)_N$, $(Ti/Zr)_N$ versus $^{143}Nd/^{144}Nd$ and $(Zr/Y)_N$ versus $(Ti/Zr)_N$ showing the compositions of Victoria's lava lake komatiitic basalts (*diamonds*) and mixing lines between an inferred komatiite parent and a crustal contaminant. (*BK* Belingwe komatiite, *UCC* upper continental crust). *Numbers* next to *tick marks* give percentage contaminant

origin of high-magnesian volcanic rocks in general, and in this volcanic pile in particular.

2. The differentiated body of komatiitic basalt studied represents an areally extensive 110 m deep lava lake. During eruption, the initial liquid had a temperature of 1380–1400 °C, contained ~ 15% MgO and ponded in a large topographic depression soon after emplacement. Evolution of the erupted magma was controlled by settling of transported olivine and chromite phenocrysts and resulted in the prominent internal layering. The last portions of the trapped liquid crystallized at 1250 to 1070 °C. As evidenced by two-pyroxene and olivine-spinel thermometry, these mineral systems were frozen between 1185–1225 and 970–1040 °C, respectively.

3. The internal Sm-Nd isochron of 2410 ± 34 Ma provides a reliable estimate for the time of formation of the uppermost sequences in the Vetreny Belt. This age is in good agreement with the Sm-Nd and Pb-Pb isochron ages of 2449 ± 35 and 2424 ± 178 Ma for the volcanic rocks from the same stratigraphic level in the Golets Hills area, northwestern Vetreny Belt.

4. Modeling of isotopes, major and trace elements can be used to show that the komatiitic basalts at Lion Hills may have had an incompatible trace element-depleted komatiite parent. This initial liquid was shown to have undergone 7–9% contamination by upper crustal rocks *en route* to the surface thus acquiring the observed geochemical and isotope signatures [relative enrichment in Zr, Ba, and LREE, negative Nb- and Ti-anomalies and negative εNd(T) value].

**Acknowledgements** The handpicking of mineral separates was carefully and patiently done by V.Pavlichenko and N.Ashikhmina. I.S.P. thanks Prof. H.A. Seck for support during microprobe work at the Mineralogisch-Petrographishes Institut in Cologne. Discussions with Dallas Abbott and Svetlana Bogdanova were most beneficial. Critical comments of Heinz Stosch, Peter Sorjonen-Ward and an anonymous reviewer substantially improved the initial draft of the manuscript. I.S.P. acknowledges the support of the Alexander von Humboldt Foundation.

## References

Abbott D, Burgess L, Longhi J, Smith WHF (1994) An empirical thermal history of the Earth's upper mantle. J Geophys Res 99:13835–13850

Arndt NT (1976) Melting relations of ultramafic lavas (komatiites) at one atmosphere and high pressure. Carnegie Inst Washington Yearb 675:555–562

Arndt NT (1986a) Komatiites: a dirty window to the Archean mantle. Terra Cognita 6:59–66

Arndt NT (1986b) Differentiation of komatiite flows. J Petrol 27:279–301

Arndt NT (1986c) Spinifex and swirling olivines in a komatiite lava lake, Munro Township, Canada. Precambrian Res 34:139–155

Chauvel C, Dupré B, Arndt NT (1993) Pb and Nd isotope correlation in Belingwe komatiites and basalts. In: Bickle MJ, Nisbet EG (eds) The geology of the Belingwe Greenstone Belt, Zimbabwe: a study of the evolution of Archaean continental crust. AA Balkema, Rotterdam, Brookfield, pp 167–174

Arndt NT, Fleet ME (1979) Stable and metastable pyroxene crystallization in layered komatiite flows. Am Mineral 64:856–864
Arndt NT, Jenner GA (1986) Crustally contaminated komatiites and basalts from Kambalda, Western Australia. Chem Geol 56: 229–255
Arndt NT, Naldrett AJ, Pyke DR (1977) Komatiitic and iron-rich tholeiitic lavas of Munro Township northeast Ontario. J Petrol 18:319–369
Beattie P, Ford C, Russell D (1991) Partition coefficients for olivine-melt and orthopyroxene-melt systems. Contrib Mineral Petrol 109:212–224
Bibikova EV, Skiöld T, Bogdanova SV (1996) Age and geodynamic aspects of the oldest rocks in the Precambrian Belomorian Belt of the Baltic (Fennoscandian) Shield. Geol Soc London Spec Publ 112 (in press)
Bogdanova SV, Bibikova EV (1993) The "Saamian" of the Belomorian mobile belt: new geochronological constraints. Precambrian Res 64:131–152
Brandon AD, Hooper PR, Goles GG, Lambert RSJ (1993) Evaluating crustal contamination in continental basalts: the isotopic composition of the Picture Gorge Basalt of the Colombia River Basalt group. Contrib Mineral Petrol 114:452–464
Campbell IH, Arndt NT (1982) Pyroxene accumulation in spinifex-textured rocks. Geol Mag 119:605–610
Cattell A (1987) Enriched komatiitic basalts from Newton Township, Ontario: their genesis by crustal contamination of depleted komatiite magma. Geol Mag 124:303–309
Chase CG, Patchett PJ (1988) Stored mafic/ultramafic crust and early Archean mantle differentiation. Earth Planet Sci Lett 91:66–72
Chauvel C, Dupré B, Jenner GA (1985) The Sm-Nd age of Kambalda volcanics is 500 Ma too old! Earth Planet Sci Lett 74:315–324
Condie KC (1989) Geochemical changes in basalts and andesites across the Archean-Proterozoic boundary: identification and significance. Lithos 23:1–18
Donaldson CH (1976) An experimental investigation of olivine morphology. Contrib Mineral Petrol 57:187–213
Donaldson CH (1982) Spinifex-textured komatiites: a review of textures compositions and layering. In: Arndt NT, Nisbet EG (eds) Komatiites. George Allen and Unwin, London, pp 213–244
Dupré B, Arndt NT (1990) Pb isotopic composition of Archean komatiites and sulfides. Chem Geol 85:35–56
Fletcher IR, Rosman KJR (1982) Precise determination of initial εNd from Sm-Nd isochron data. Geochim Cosmochim Acta 46:19–22
Gaál G, Gorbatschev R (1987) An outline of the Precambrian evolution of the Baltic Shield. Precambrian Res 35:15–52
Galer SJG, Goldstein SL (1991) Early mantle differentiation and its thermal consequences. Geochim Cosmochim Acta 55:227–239
Glazner AF, Farmer GL (1992) Production of isotopic variability in continental basalts by cryptic crustal contamination. Science 255:72–74
Gole MJ, Barnes SJ, Hill RET (1990) Partial melting and recrystallization of Archean komatiites by residual heat from rapidly accumulated flows. Contrib Mineral Petrol 105:704–714
Gorbatschev R, Bogdanova S (1993) Frontiers in the Baltic Shield. Precambrian Res 64:3–21
Green TH (1994) Experimental studies of trace-element partitioning applicable to igneous petrogenesis – Sedona 16 years later. Chem Geol 117:1–36
Hanson GN, Langmuir CH (1978) Modelling of major elements in mantle-melt systems using trace element approaches. Geochim Cosmochim Acta 42:725–741
Hart SR, Dunn T (1993) Experimental cpx/melt partitioning of 24 trace elements. Contrib Mineral Petrol 113:1–8
Hart SR, Zindler A (1986) In search for bulk-earth composition. Chem Geol 57:247–267
Helz RT, Kirschenbaum H, Marinenko JW (1989) Diapiric transfer of melt in Kilauea Iki lava lake Hawaii: a quick efficient process of igneous differentiation, Geol Soc Am Bull 101:578–594
Herbert R (1982) Petrography and mineralogy of oceanic peridotites and gabbros: some comparisons with ophiolite examples. Ofioliti 7:299–324
Hofmann AW (1988) Chemical differentiation of the Earth: the relationship between mantle, continental crust and oceanic crust. Earth Planet Sci Lett 90:297–314
Huppert HE, Sparks RSJ (1985) Cooling and contamination of mafic and ultramafic magmas during ascent through continental crust. Earth Planet Sci Lett 74:371–386
Huppert HE, Sparks RSJ, Turner JS, Arndt NT (1984) Emplacement and cooling of komatiite lavas. Nature 309:19–22
Jacobsen SB, Wasserburg GJ (1980) Sm-Nd isotopic evolution of chondrites. Earth Planet Sci Lett 50:139–155
Jacobsen SB, Wasserburg GJ (1984) Sm-Nd isotopic evolution of chondrites and achondrites. II. Earth Planet Sci Lett 67:137–150
Jan MQ, Windley BF (1990) Chromian spinel – silicate chemistry in ultramafic rocks of the Jijal complex, northwest Pakistan. J Petrol 31:667–715
Jochum KP, Arndt NT, Hofmann AW (1991) Nb–Th–La in komatiites and basalts: constraints on komatiite petrogenesis and mantle evolution. Earth Planet Sci Lett 107:272–289
Kinzler RJ, Grove TL (1985) Crystallization and differentiation of Archean komatiite lavas from northeast Ontario: phase equilibrium and kinetic studies. Am Mineral 70:40–51
Kulikov VS (1971) Volcanic rocks in the Vetreny Belt range. In: Sidorenko AV (ed) Problems of the Precambrian sedimentary geology. Nedra, Moscow, pp 253–265
Kulikov VS (1983) The Proterozoic. In: Krats KO (ed) Earth's crust and metallogeny in the southeastern part of the Baltic shield. Nauka, Leningrad, pp 32–40
Kulikov VS (1988) High-magnesian volcanism in the early Proterozoic. In: Bogatikov OA (ed) Komatiites and high-magnesian volcanic rocks in the early Precambrian of the Baltic Shield. Nauka, Leningrad, pp 20–88
Kulikov VS, Kalinin YK (1971) Experimental reproduction of some textures in basalts from the Vetreny Belt. In: Nalivkin AB (ed) Mineralogy and geochemistry of Karelia. Nauka, Leningrad, pp 168–172
Kulikov VS, Simon AK, Kulikova VV, Samsonov AV, Kajrjak AI, Ganin VA, Zudin AI (1990) Evolution of Archean magmatism in the Vodla Block, Karelian granite-greenstone terrane. In: Lobach-Zhuchenko SB, Bibikova EV (eds) Precambrian geology and geochronology of the East European Platform. Nauka, Leningrad, pp 92–100
Lehmann J (1983) Diffusion between olivine and spinel: application to geothermometry. Earth Planet Sci Lett 64:123–138
Lesher CM, Arndt NT (1995) REE and Nd isotope geochemistry, petrogenesis and volcanic evolution of contaminated komatiites at Kambalda, Western Australia. Lithos 34:127–158
Lindsley DH (1983) Pyroxene thermometry. Am Mineral 68: 477–493
Lobach-Zhuchenko SB, Chekulaev VP, Sergeev SA, Levchenkov OA, Krylov IN (1993) Archean rocks from southeastern Karelia (Karelian granite-greenstone terrain). Precambrian Res 62:375–397
Lofgren G, Donaldson CH, Williams RJ, Mullins O, Usselman TM (1974) Experimentally reproduced textures and mineral chemistry of Apollo 15 quartz normative basalts. Abstr Proc Fifth Lunar Sci Conf: 549–567
McDonough WF (1990) Constraints on the composition of the continental lithospheric mantle. Earth Planet Sci Lett 101:1–18
McDonough WF, Sun S-s (1995) The composition of the Earth. Chem Geol 120:223–253
McRae ND, Russell MR (1987) Quantitative REE SIMS analyses of komatiite pyroxenes, Munro Township, Ontario, Canada. Chem Geol 64:307–317
Nesbitt RW (1971) Skeletal crystal forms in the ultramafic rocks of the Yilgarn Block, Western Australia: evidence for an Archean ultramafic liquid. Geol Soc Aust Spec Publ 3:331–347

Nisbet EG, Arndt NT, Bickle MJ, Cameron WE, Chauvel C, Cheadle M, Hegner E, Kyser TK, Martin A, Renner R, Roedder E (1987) Uniquely fresh 2.7 Ga komatiites from the Belingwe greenstone belt, Zimbabwe. Geology 15:1147–1150

Nisbet EG, Cheadle MJ, Arndt NT, Bickle MJ (1993) Constraining the potential temperature of the Archean mantle: a review of the evidence from komatiites. Lithos 30:291–307

Puchtel IS, Zhuravlev DZ, Kulikov VS, Kulikova VV (1991) Petrography and Sm-Nd age of a komatiitic basalt differentiated flow in the Vetreny Belt, Baltic Shield. Geochem Int 28(12):14–23

Renner R, Nisbet EG, Cheadle MJ, Arndt NT, Bickle MJ, Cameron WE (1994) Komatiite flows from the Reliance Formation, Belingwe Belt, Zimbabwe. I. Petrography and mineralogy. J Petrol 35:361–400

Roeder PL, Emslie RF (1970) Olivine-liquid equilibrium. Contrib Mineral Petrol 29:275–282

Rudnick RL, Fountain DM (1995) Nature and composition of the continental crust: a lower crustal perspective. Rev Geophys 33:267–309

Ryabchikov ID, Suddaby P, Girnis AV, Kulikov VS, Kulikova VV, Bogatikov OA (1988) Trace-element geochemistry of Archean and Proterozoic rocks from eastern Karelia, USSR. Lithos 21:183–194

Slyusarev VD, Kulikov VS (1973) Geochemical evolution of Proterozoic basic-ultrabasic magmatism in the southeastern Baltic Shield. Nauka, Leningrad

Sokolov VA (ed) (1987) Geology of Karelia. Nauka, Leningrad

Thirlwall MF (1982) A triple-filament method for rapid and precise analysis of rare earth elements by isotope dilution. Chem Geol 35:155–166

Thy P (1995) Low-pressure experimental constraints on the evolution of komatiites. J Petrol 36:1529–1548

Timmerman MJ, Daly JS (1995) Sm-Nd evidence for late Archean crust formation in the Lapland-Kola Mobile Belt, Kola Peninsula, Russia and Norway. Precambrian Res 72:97–107

Turner JS, Huppert HE, Sparks RSJ (1986) Komatiites. II. Experimental and theoretical investigations of post-emplacement cooling and crystallization. J Petrol 27:397–437

Wright TL, Kinoshita WT, Peck DL (1968) March 1965 eruption of Kilauea Volcano and the formation of Makaopuhi lava lake. J Geophys Res 73:3181–3205

York D (1966) Least squares fitting of straight line. Can J Phys 44:1079–1086

Zhou M, Kerrich R (1992) Morphology and composition of chromite in komatiites from the Belingwe greenstone belt, Zimbabwe. Can Mineral 30:303–317

Zhuravlev DZ, Puchtel IS, Samsonov AV (1989) Sm-Nd age and geochemistry of metavolcanic rocks from the Olondo greenstone belt, Aldan Shield. Izv Akad Nauk SSSR Ser Geol 2: 39–49